Energy management for hybrid and fully electric vessels via a multi-objective Equivalent Consumption Minimization Strategy

Löffler, Charlotte; Geertsma, Rinze; Polinder, Henk; Coraddu, Andrea

DOI
10.1016/j.enconman.2025.120150

Publication date
2025

Document Version
Final published version

Published in
Energy Conversion and Management

Energy Conversion and Management 343 (2025) 120150

Contents lists available at ScienceDirect

Energy Conversion and Management

journal homepage: www.elsevier.com/locate/enconman

Research paper

Energy management for hybrid and fully electric vessels via a multi-objective Equivalent Consumption Minimization Strategy

Charlotte Löffler [a,*], Rinze Geertsma [b,a], Henk Polinder [a], Andrea Coraddu [a]

[a] Delft University of Technology, Delft, Netherlands
[b] Netherlands Defense Academy, Den Helder, Netherlands

ARTICLE INFO

Keywords:
Energy management
Full-electric vessel
Multi-objective control
Optimization
ECMS
NO_x emission
Hydrogen

ABSTRACT

A key factor towards zero-emission shipping is the adoption of electric propulsion with hybrid power sources. The heterogeneous power sources of modern electric vessels require optimal energy management systems, as conventional rule-based control in hybrid energy systems may result in suboptimal solutions with limited flexibility. Advanced optimal control strategies offer a promising avenue to address this issue. This paper presents a novel control strategy based on the Equivalent Consumption Minimization Strategy for a dual-fuel full-electric vessel operating with diesel engines and hydrogen fuel cells taking into account both fuel cost and NO_x emissions. The effectiveness of the developed controllers is evaluated against a benchmark derived from state-of-the-art strategies in a simulation study using real-world data. The results highlight the controller's performance, as well as the operator's choice by selection of weights for the objectives. The proposed control strategy achieves nearly 2 % fuel savings compared to a single-objective rule-based controller. It also exploits the potential for up to 45 % reductions in NOx emissions. When both objectives are combined, the controller still delivers over 0.5 % fuel savings while reducing NOx emissions by nearly 15 %. If a financial cost is assigned to emissions, the total operational cost savings increase to more than 4 %.

1. Introduction

Facing the dangers of climate change, a reduction in the green house gas emissions of the shipping sector is required to meet the goals of the Paris Agreement [1,2]. Despite efforts of the International Maritime Organization (IMO), annual CO_2 emissions from shipping are close to 3 % of total greenhouse gas emissions, and expected to grow further [3–5]. Moreover, shipping contributes significantly to acidification of the ocean and coastal regions, global sulfur loading, and increased ozone perturbation in summer months with its hazardous emissions [6–8]. While some of the relevant emissions, such as CO_2 and sulfur, are related to fuel consumption and the fuel itself [5], other emissions, prominently Nitrogen Oxide (NO_x), Particulate Matter (PM) and methane, depends more on the power source, which currently typically consists of Internal Combustion Engines (ICE), and its operational point. A transition to alternative fuels, such as hydrogen, alternative power sources, such as fuel cells, and energy storage (ES) technologies, such as batteries to change the power source operating point, can reduce these emissions [9].

This transition towards a sustainable maritime industry first requires electric propulsion to enable easier integration of alternative power sources and ES on ships [10]. Replacement of a separate mechanical propulsion and electrical power system with an integrated electrical power system on board the ship for propulsion and electrical power supply allows the integration of a wide variety of power sources and ES components [11]. This results in increased operational flexibility and enables the potential for energy and emission savings [9, 12]. Batteries offer a zero-emission solution for battery-electric ship propulsion [13]. However, their application is currently limited to short travel distances due to the relatively low energy density of battery systems [14]. While extending voyage range using batteries alone remains challenging, they have been shown to significantly reduce emissions during port operations and at berth [15].

To enable those longer travel distances, alternative fuels should be considered [13]. A number of studies have investigated the application of alternative fuels both in the general energy sector [16] and specifically in the maritime sector [17–21]. Initial design feasibility studies further suggest that LNG is a promising candidate for real-world vessel applications [22]. As hydrogen is specifically suitable for high-temperature industrial processes, its availability for fuel application might be limited in the short term, according to the complete energy

* Corresponding author.
E-mail address: c.loeffler@tudelft.nl (C. Löffler).

https://doi.org/10.1016/j.enconman.2025.120150
Received 23 April 2025; Received in revised form 17 June 2025; Accepted 1 July 2025
Available online 24 July 2025

Nomenclature

A	Tafel slope
C	cost function objective
E	Battery no-load voltage
E_0	generator no-load voltage
F	Faraday constant
I_a	line current
I_f	field current
I_{a1}	armature current phasor
I_{ad}	armature current phasor
J	optimization problem solution
K	battery polarization voltage
N	number of fuel cells in series
P_1	generator active power
P_J	Joule losses
P_L	generator load power
P_{Aux}	auxiliary power load
P_{Bat}	battery power
P_{Eng}	engine power
P_{FC}	fuel cell power
$P_{\text{F\&W}}$	friction and windage losses
P_{Hotel}	hotel power load
P_{Load}	total power load
P_{Prop}	propulsion power load
P_{core}	core losses
$P_{\text{no-load}}$	generator no-load power
P_{shaft}	shaft power
P_r	power loss in rotor resistance
Q	battery capacity
Q_1	generator reactive power
Q_L	reactive power consumed by load
Q_{nom}	battery nominal capacity
R	resistance
$R_{\text{Bat,int}}$	battery internal resistance
$R_{\text{FC,int}}$	battery internal resistance
R_a	stator winding resistance
T_{shaft}	shaft torque
T_{em}	electromagnetic torque
V_1	line phase voltage
V_{Bat}	battery voltage
V_{DC}	DC bus voltage
V_{FC}	fuel cell voltage
X_s	synchronous reactance
X_{sd}	d-axis synchronous reactance
X_{sq}	q-axis synchronous reactance
Δt	sampling rate
Θ	formation rate
$\Theta_{\text{NO}_x,\text{Eng}}$	engine NOx formation rate
$\Theta_{\text{SFC,Eng}}$	engine fuel consumption rate
δ	torque angle
η_{AC-DC}	AC-DC conversion efficiency
η_{DC-AC}	DC-AC conversion efficiency
η_{DC-DC}	DC-DC conversion efficiency
η_{gb}	gearbox loss
η_m	motor efficiency
η_{sg}	generator efficiency
λ	objective weight
ω	synchronous speed
ϕ_a	power angle
ρ	density
ζ	battery equivalence factor
i_{Bat}	battery current
i_{Eng}	current produced by engine
i_{FC}	current produced by fuel cell
i_{Hotel}	hotel load current
i_{Load}	total load current
i_{Prop}	propulsion load current
k	time step of the control problem
m_{D}	mass of diesel fuel consumed
m_{NO_x}	mass of NOx emission produced
n_{Eng}	engine speed
n_p	battery cells in parallel
n_s	battery cells in series
p_D	price diesel
p_{Bat}	battery price
p_{H2}	price hydrogen
r_{CO2}	release rate CO2
u	control variable
x	state variable
z	number of moving electrons
AC	Alternating Current
AS	Active Set
DC	Direct Current
ECMS	Equivalent Consumption Minimization Strategy
ES	Energy Storage
FC	Fuel Cell
GA	Genetic Algorithm
ICE	Internal Combustion Engine
IMO	International Maritime Organization
IP	Interior Point
MI	Mixed Integer
MPC	Model Predictive Control
NL	Non Linear
NOx	Nitrogen Oxide
PEMFC	Proton Exchange Membrane Fuel Cell
PM	Particulate Matter
PS	Pattern Search
RBC	Rule Based Control
SFC	Specific Fuel Consumption
SOC	State of Charge
SQP	Sequential Quadratic Programming

sector review in [16]. For the maritime sector, [23] identifies the factors that need to be resolved to apply alternative fuels in shipping, ranging from technology readiness to fuel availability. Subsequently, Deniz et al. [18,19] conclude that economically liquefied natural gas is the most suitable fuel to reduce hazardous emissions in the short term, but hydrogen can be the future fuel of choice for ships to reduce greenhouse gas emissions and achieve zero-emission propulsion and power supply.

On the other hand, hydrogen and FCs are costly and availability of hydrogen is limited, restricting their application potential [16].

Combining hydrogen FCs with diesel ICEs presents a first step towards emission and noise reduction during operations at low power, while still being able to economically deal with high propulsion loads. Moreover, ICE emissions can be reduced by choosing the operating point, especially when applied with electric propulsion and DC hybrid power supply [11]. In the engine envelope, the specific fuel consumption (SFC) and emissions change based on the delivered torque and engine speed. The CO_2 emissions are directly related to the SFC with a carbon factor that depends on the fuel, while NO_x emissions depend on the local temperature of combustion in the cylinder, which is driven by the charge air pressure, engine speed and amount of injected fuel [24,25]. Therefore, actively determining an optimal setpoint for engine speed and power allows a more conscious choice regarding fuel consumption and emissions.

A DC power system provides the control freedom to choose engine speed to achieve the best fuel consumption or emissions for the required power [11]. Thus, the control mechanism must navigate a delicate balance when incorporating a dual-fuel system. The choice between using diesel, a cost-effective fuel with associated CO_2 and NO_x emissions, and hydrogen, a cleaner but more expensive option, presents a significant trade-off. Coupling these power sources with an ES system like batteries offers benefits such as buffering against load variations, achieving peak shaving, and allowing the ICE and fuel cells to run at an operating point with higher efficiency and less emissions [26]. However, these possibilities allow for the introduction of additional objectives into the operation of the energy system. Commonly, the main objective of the operation is an economic one, relating to the respective reduction of fuel consumption and therefore operational costs. With the efforts to reduce the carbon footprint of the maritime sector, the reduction of emissions is gaining interest as an objective. In addition, with the introduction of new components, such as batteries or FC, the objective to reduce component degradation is becoming more and more important. All those objectives have different optimal points for operating the components of the energy system, resulting in an operator's choice problem to determine the compromise between them. As a result, the energy system operation evolves into a multi-objective optimization problem that demands a real-time solution when trying to achieve optimality.

This multi-objective optimization is a challenge for the commonly used rule-based control (RBC), as it often leads to suboptimal solutions [27]. RBC approaches have been shown to achieve good performance in their design conditions, but can significantly drop in performance when dealing with a different operating profile or uncertainties such as changing weather conditions [28]. A solution to address this increased complexity of the control problem is an advanced control approach [29]. Advanced control strategies have undergone previous investigation in marine energy management in recent years.

A notable approach to improve energy efficiency in diverse application domains with predictable operating profiles is Model Predictive Control (MPC) [30–35]. In automotive, MPC approaches have been used to determine the sub-optimal power-split between a single battery system and the ICE of a vehicle, mostly for energy efficiency [31–33,36], but also for multiple objectives [34] or to introduce alternative fuel systems [37]. Johannesson et al. [31] propose a predictive control scheme for energy management with a convex optimization approach to establish the sub-optimal control for the management of electric and kinetic energy for autonomous long-haul trucks. They demonstrate fuel savings due to autonomous speed control on trajectories with small to medium differences in altitude. The future propulsion load can be established, because the autonomous vehicle can plan its future speed and load profile based on geographic and route planning information. Unger et al. [32] demonstrate that short-term prediction based on Bayesian inference can be used to improve energy efficiency and reduce engine dynamics, when the driver determines the speed profile. Kermani et al. [33] have developed an approach that does not require control freedom of the future vehicle speed. They propose a strategy that uses prediction of the distribution of future driving conditions and an underlying Equivalent Consumption Minimization Strategy (ECMS) to establish a real-time control strategy with an embedded off-line optimization that takes driving conditions in the nearby future into account. They show that a compromise between fuel consumption and battery use can be achieved in a use case on a trajectory without altitude differences. Finally, Pozzato et al. [34] propose an economic MPC approach to optimize over multiple objectives, such as fuel consumption, battery aging and noise emissions. This approach achieves convergence to the optimum for a convex problem formulation and can be used to solve energy management computationally efficiently for on-board energy management and sizing problems. However, real-time approaches require a definition of convex optimization problems.

In shipping, MPC exhibits versatility in energy management with various objectives [38]. A first study from Jiang et al. [39] shows the potential of MPC for real-time control of alternatively fueled vessels. The authors show the fuel saving and degradation reduction enabled by the combination of load forecasting and economic MPC for a small boat using PEMFC. The authors require a large amount of knowledge and data to be able to determine the load forecast, which remains unfeasible for many vessels currently. However, a significant challenge associated with MPC is the required knowledge about future operation of the system to accurately predict system behavior, which is time- and cost-intense [40]. While in the automotive sector, typical load profiles — such as acceleration, cruising, and braking — can be predicted with reasonable accuracy based on standardized drive cycles and road conditions, maritime operations present a far greater challenge. At sea, load demand is influenced by a highly variable and often unpredictable environment, including wind, waves, currents, and vessel maneuvering dynamics. These external factors introduce significant fluctuations in propulsion and auxiliary power requirements, making it difficult to accurately forecast the system load over time. This uncertainty complicates the implementation of energy management strategies and optimal control schemes in marine applications.

This challenge becomes particularly pronounced for vessels characterized by high uncertainty in their load profiles, making the application of MPC even more complex. Therefore, advanced control approaches, which require less extensive knowledge about system behavior and load profile, are more suitable for uncertain operations in the maritime, such as the ECMS.

ECMS is an instantaneous optimization strategy commonly employed to successfully operate heterogeneous energy systems across differently-natured energy sources such as ICEs, FCs, and batteries [41]. Inherently, ECMS establishes correlations among objectives through an equivalent factor for battery use within its objective function. This correlation empowers the control mechanism to achieve an optimal balance among energy sources of a diverse nature. Because it only optimizes one-time step ahead, which offers computational savings compared to MPC, the application is easier to control in real-time.

ECMS is already widely explored in other areas of transport research [42–49], most prominently the automotive. Already in 2011, Torreglosa et al. [42] show the successful power splitting of ECMS for fuel consumption reduction in the application of a FC-battery-electric tramway. Similarly, Zhang et al. [43] develop an ECMS control for a PEMFC tramway incorporating also batteries and supercapacitors. The control manages to successfully minimize the fuel consumption while operating with and without grid connection. In the automotive, Li et al. [46] present a SQP-based ECMS strategy for the fuel consumption reduction of a FC-electric vehicle. The authors show that it is possible to reduce the hydrogen consumption in comparison to a rule-based benchmark and to stabilize the FC current to contribute to a healthy operational approach. Nuesch et al. [50] use ECMS to reduce the real driving NO_x emissions of a diesel-electric vehicle. By determining the optimal power split the battery is used to reduce the emission production of the engine. The authors show the effectiveness of their approach to reduce fuel consumption and NO_x emissions using

Hardware-in-the-Loop experiments. In 2020, Li et al. [51] explore the selection of the optimal equivalent factor further. The authors present an analytical expression of the boundary for the optimal choice based on the Hamilton equation of PMP.

While this research confirms the promising potential ECMS for optimal power distribution among heterogeneous energy sources, several critical challenges arise when transitioning from automotive to maritime applications. Maritime power systems are orders of magnitude larger, as they incorporate diverse power sources and are often more complex than those in automotive settings, primarily due to the substantial and fluctuating power demands required for propulsion and auxiliary operations across various vessel types. This drastically increases the dimensionality and computational burden of the optimization problem. Unlike automotive systems, where ECMS typically manages the power split between a single primary energy source and a storage unit [47], maritime applications must coordinate multiple energy sources and storage systems simultaneously, often with differing dynamic and efficiency characteristics [27]. Furthermore, the conventional use of constant equivalent factors in ECMS becomes inadequate in maritime contexts, where operating conditions and component performance can vary widely. Although adaptive equivalent factors can address this issue by dynamically adjusting to system changes, they also introduce additional computational complexity and tuning challenges. These expanded and highly nonlinear optimization problems demand more advanced solution methods and significantly longer computation times. Successfully implementing ECMS in the maritime domain, therefore, requires rethinking its control architecture, with particular attention to scalability, adaptability, and robustness under real-world marine operating conditions.

In a pioneering maritime application, Kalikatzarakis et al. [28] highlighted the fuel-saving capabilities of ECMS for vessels in a single-objective optimization. For this, the authors use a convex model, which allows for a fast problem solution. However, integrating differently-natured objectives, such as emissions different from CO_2 or component aging, warrants further exploration as these other emissions typically do not allow for a convex problem definition. In 2023, Löffler et al. investigated ECMS for a multi-objective problem in a full-electric vessel in two small studies [52,53]. However, those studies took into account only a concise operational time frame to provide a proof of concept, which is insufficient to fully establish the benefits of the ECMS approach. Expanding this study and taking into account a longer operational profile, a system model with higher accuracy, and a further developed optimization problem will provide more insights into the efficiency of this method compared to commonly used strategies in the field, such as RBC. As discussed in the previous, most ECMS approaches use a constant equivalent factor to compare between the different forms of energy [28,33]. Transitioning towards adaptive factors in maritime ECMS is an open gap to incorporate the complexity of the energy system and enable the control to flexibly adapt to the changing conditions of an operation.

This paper presents a novel multi-objective ECMS approach for the energy management of a dual-fuel full-electric vessel, taking into account both the fuel consumption of two intrinsically different fuels and of NO_x emissions. Based on this, the novelty of this work can be defined as follows:

- The paper proposes a real-time multi-objective ECMS method to deal with the energy management problem of a dual-fuel fully electric vessel with hybrid power supply integrating ICE, FC and batteries, which translates into a mixed-integer non-convex problem.
- The proposed ECMS with an adaptive equivalent factor for battery usage can optimize the power split between the components under changing operational conditions and for multiple objectives, allowing a trade-off between fuel cost, CO_2 emissions, and NO_x emissions.

Table 1
Case study vessel specification.

Specification	Parameter
Length	87 m
Beam	13.5 m
Draught	3.9 m
Displacement	2470 t
GT volume	3000 t
Max. Speed	18 kn
Range	5000 nm
Max propulsion power	4000 kW
Max auxiliary power	1000 kW
Mean auxiliary load	280 kW

Table 2
Case study vessel user profile.

Mode	Frequency [%]
Sailing	10
At anchor	33
In harbour	57

- The potential for emission saving by introducing zero-emission fuel against a common industry benchmark using both rule-based and advanced control is quantified.

The paper is structured as follows: In Section 2, the chosen use case for this study is outlined by introducing the vessel and the virtual retrofit. Section 3, the methodology section, explains both the simulation model and the optimization problem. Section 4 introduces the simulation study, as well as the benchmark RBC. In Section 5, the results are analyzed and discussed for the chosen objectives. Last, the findings are summarized in Section 6.

2. Use case

The use case for this study is a yacht with electric propulsion and hybrid power supply, with a combination of a diesel engine, hydrogen fuel cells and a battery ES. This power source configuration allows for a trade-off between low emissions and noise, specifically at low power transit or anchored operations, and cost, specifically for high-speed operation. The specifications of the case study vessel are reported in Table 1. The original layout of four diesel generators and an AC shipboard power grid is a typical full-electric vessel layout, which will be considered as industry benchmark in the study. The load profile of a yacht usually contains both hotel and propulsion loads, while fulfilling the hotel loads is a key aspect of the operation. An overview of the typical user profile over time is described in Table 2.

10 000 h of real-world operational data from a typical yacht with electric propulsion and diesel engine power system are obtained. The operational data are shown in Fig. 1. The auxiliary load is shown in red, while the propulsion load is shown in blue. The first plot of the figure shows the complete 10 000 h of the operational data, while the third plot shows the histogram of relative frequencies (excluding zeros). This data illustrates that the most common and frequent loads are the auxiliary systems with limited variation in the requested electric load. In contrast, the propulsion load occurs at much lower frequencies, and the spread of the requested load is larger. Generally, when propulsion load occurs, the yacht is sailing or manoeuvring.

However, the data show that the nature of these sailing trips is very diverse. This is illustrated in the second plot of Fig. 1. The second plot is split into three different cut-outs from the first plot, all three illustrating different trips. The first trip shows a consecutive use of 5 days. Alternatively, the second plot shows 6 weeks of use, with a short period without propulsion load in the middle. Finally, the third plot illustrates shorter periods of use, mainly about a day long. A vessel of this type can be expected to perform longer sailing trips in the

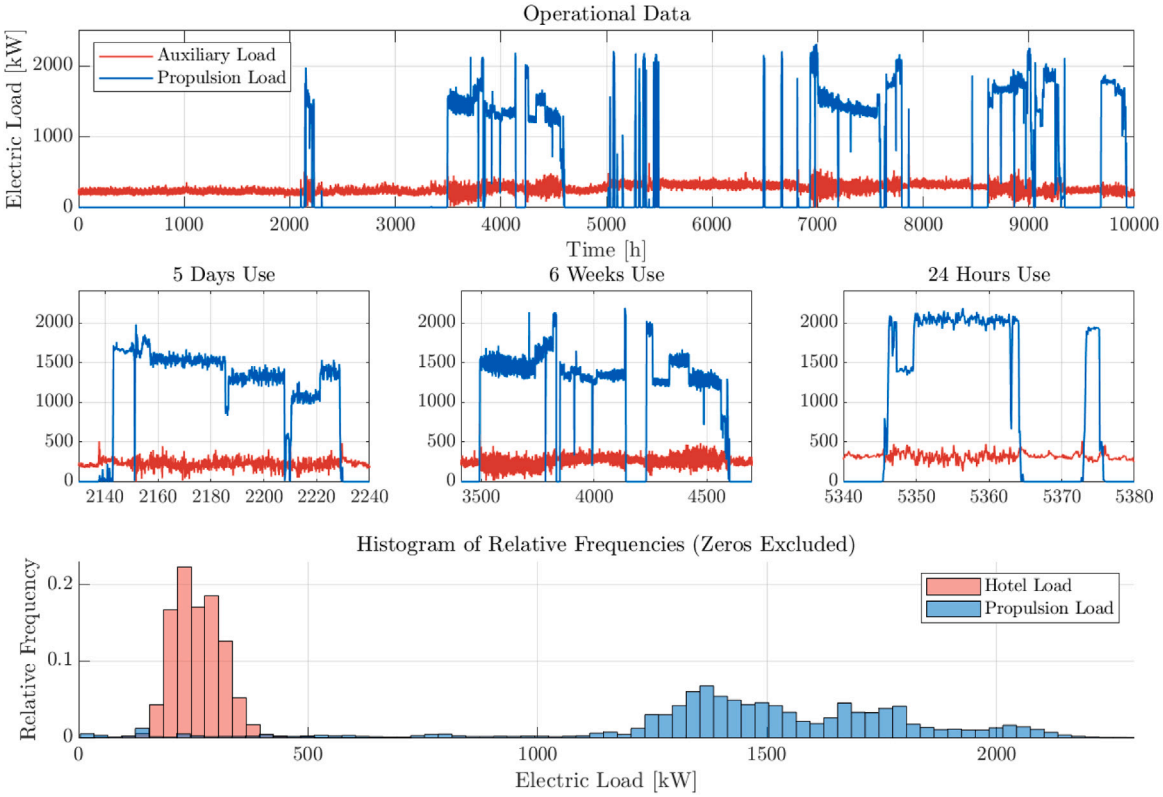

Fig. 1. Operational data from the case study vessel covering 10 000 h and histogram of relative frequencies for the electric load.

summer season and in regions with high temperatures, while often in the harbour or at anchor from autumn to spring. In addition, there will be shorter cruises or transfers when the vessel needs to be relocated. As visible from the operational data, day tours can also occur, for example in weekends. Furthermore, the amount of propulsion load varies between trips. Concluding, this operational data clearly illustrates that the energy management of such a vessel needs to be able to deal with a high amount of variation in the load demand for propulsion load while reliably providing the constant demand of auxiliary loads. From this operational data, an exemplary trip to showcase the effectiveness of the proposed controller in a simulation study can be selected.

For this use case, the vessel is retrofitted to accommodate a dual-fuel system, introducing hydrogen as a zero-emission fuel into the power train. For this, the retrofitted version replaces two of the original engines in the vessel energy system with hydrogen Proton Exchange Membrane Fuel Cells (PEMFC). These are accompanied by two diesel ICE and two battery packs. This dual-fuel layout enables the reduction of fossil fuel consumption by replacing some power sources with zero-emission fuel-cells. Other options for a retrofit, such as battery-electric or battery-FC-only combinations, are less feasible for the required load profile due to weight limits, tank size and space requirements. For the retrofit, the analysis of the load profile in Fig. 1 is taken into account. It is observable that the most frequent loads requested are hotel loads in a range between 200 kW and 400 kW. The efficiency of the PEMFC in this retrofit is best at low loads, which makes it desirable to use them to supply a steady base load. Furthermore, FCs are heavily affected by degradation under fast load changes, so the dynamics of the load profile are buffered by the batteries and engines. Therefore, each FC is sized to a power rating of 215 kWe, which allows all four FCs to constantly provide sufficient power for the hotel loads while staying in a good efficiency range. This is combined with the ICEs, which have a power rating of 1430 kWe to be able to provide the required propulsion loads. The addition of two battery packs with a nominal capacity of 2250 kW h allows for buffering of small load changes and can maintain the FCs

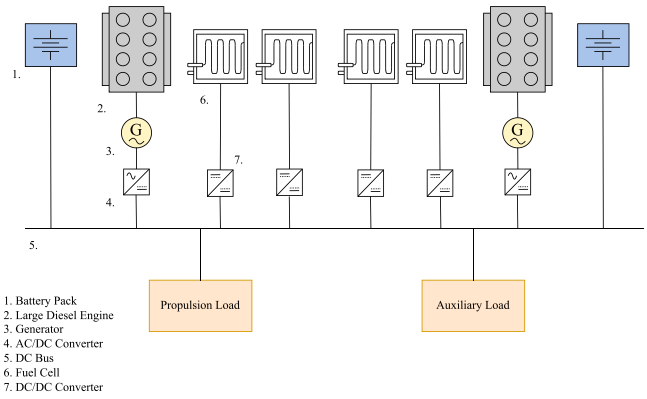

Fig. 2. Retrofitted layout of the yacht.

at continuous load levels, which is beneficial for both efficiency and component degradation [54]. The shipboard power system operates on DC with the battery connected directly to the DC bus. While the four fuel cells are connected using DC/DC converters, the ICE is combined with generators and an AC/DC conversion. This configuration allows for the use of engines at variable speed, allowing additional freedom in the control. The power system layout of the vessel is shown in Fig. 2 and the case study parameters are shown in Table 3.

3. Methodology

This section discusses the development of the simulation model for control testing and the development of the ECMS control approach. Subsequently, the complexity of the optimization problem is discussed and an adequate approach for solving the problem real-time is determined. Finally, the hierarchical control layout is presented. The

Table 3
Power system design of the case study.

Parameter	Description	Value
V_{DC}	DC-bus voltage	800 –-1000 V
P_{Eng}	Engine power rating (x2)	1430 KWe
P_{FC}	FC power rating (x4)	215 KWe
Q_{nom}	Battery nominal capacity (x2)	2250 KWh
η_{AC-DC}	Conversion efficiency	0.98
η_{DC-AC}	Conversion efficiency	0.98
η_{DC-DC}	Conversion efficiency	0.98
η_m	Motor efficiency	0.97
η_{gb}	Gearbox loss	0.97

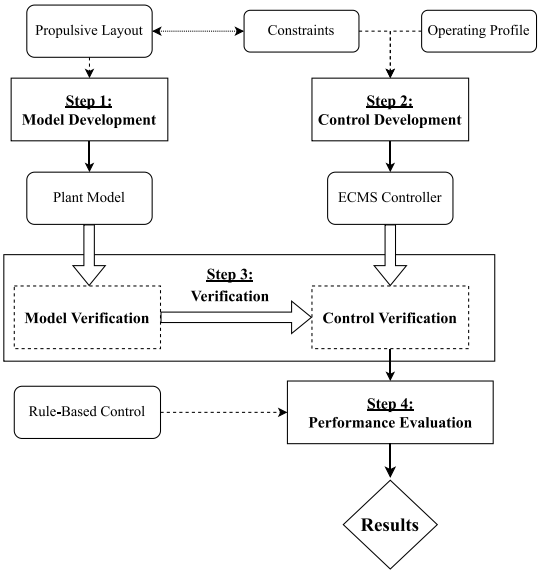

Fig. 3. Graphical abstract of the methodology.

overview of this methodology is presented as a graphical abstract in Fig. 3.

3.1. Model development

The simulation model of the physical system is developed using a single differential equation for battery state of charge (SOC) and mathematical relations of steady-state behavior, as research confirmed that steady state models are sufficiently accurate to establish fuel consumption over true operating profiles [55,56]. These models are calibrated with real-world measurements to accurately represent fuel consumption and emissions. The charging and discharging of the battery system and the state of charge (SOC) of the battery is the single state in the proposed modeling approach, as the SOC and the discharge current drive the losses in the battery [57] The causal relations for the model are illustrated in Fig. 4. Major parts of the energy system model of the vessel consist of available models from the literature, which have already been validated. The model is implemented in a Simulink environment based on Matlab R2022b.

3.1.1. DC bus

The central element of the simulation model is the representation of the DC bus represented by Kirchhoff's current law, assuming the network capacitance does not influence system energy efficiency over a longer period of time, as follows:

$$\sum i(t) = \sum_{k=1}^{2} i_{\mathrm{Eng,k}}(t) + \sum_{j=1}^{4} i_{\mathrm{FC,j}}(t) - i_{\mathrm{Load}}(t) - i_{\mathrm{Bat}}(t) = 0, \tag{1}$$

with the time-dependent currents $i_{\mathrm{Eng,i}}(t)$ for the ICEs, $i_{\mathrm{FC,i}}(t)$ for the FCs, $i_{\mathrm{Load}}(t)$ for the requested load, and $i_{\mathrm{Bat}}(t)$ for the battery. The DC

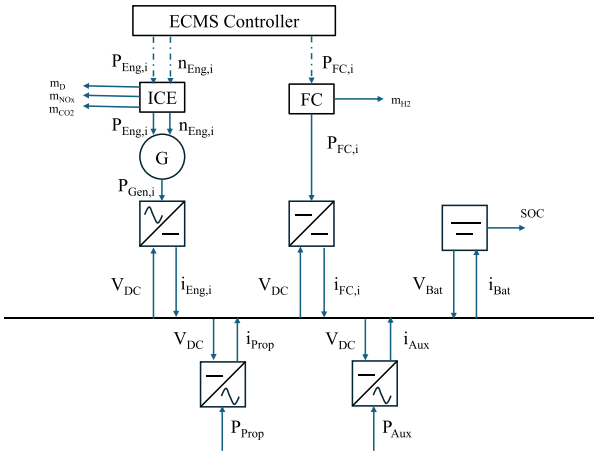

Fig. 4. Causal diagram of the simulation model and the ECMS controller.

voltage of the system V_{DC} is determined by the battery voltage V_{Bat} at all times, as the batteries are directly connected to the bus:

$$V_{\mathrm{DC}}(t) = V_{\mathrm{Bat}}(t), \tag{2}$$

The currents of the requested load and the power generation components are derived from the respective power set points and the requested power demand as follows:

$$i_{\mathrm{Eng}}(t) = \frac{P_{\mathrm{Eng}}(t)}{V_{\mathrm{DC}}(t)} \cdot \frac{\eta_{\mathrm{gen}}}{\eta_{\mathrm{AC-DC}}} \tag{3}$$

$$i_{\mathrm{FC}}(t) = \frac{P_{\mathrm{FC}}(t)}{V_{\mathrm{DC}}(t)} \cdot \eta_{\mathrm{DC-DC}} \tag{4}$$

$$i_{\mathrm{Prop}}(t) = \frac{P_{\mathrm{Prop}}(t)}{V_{\mathrm{DC}}(t)} \cdot \frac{1}{\eta_{\mathrm{gb}} \cdot \eta_{\mathrm{m}} \cdot \eta_{\mathrm{DC-AC}}} \tag{5}$$

$$i_{\mathrm{Hotel}}(t) = P_{\mathrm{Hotel}}(t) \cdot \frac{1}{\eta_{\mathrm{DC-AC}}} \tag{6}$$

$$i_{\mathrm{Load}}(t) = i_{\mathrm{Prop}}(t) + i_{\mathrm{Hotel}}(t) \tag{7}$$

$$i_{\mathrm{Bat}}(t) = i_{\mathrm{Eng}}(t) + i_{\mathrm{FC}}(t) - i_{\mathrm{Load}}(t) \tag{8}$$

where $i_{\mathrm{Eng}}(t)$ and $i_{\mathrm{FC}}(t)$ describe the diesel generator and FC current, $i_{\mathrm{Prop}}(t)$ and $i_{\mathrm{Hotel}}(t)$ are the currents of the hotel and propulsion load, which are later combined to an overall load current $i_{\mathrm{Load}}(t)$. The resulting battery current $i_{\mathrm{Bat}}(t)$ is the difference between the generated and the consumed load, as follows:

$$i_{\mathrm{Bat}}(t) = i_{\mathrm{Eng}}(t) + i_{\mathrm{FC}}(t) - i_{\mathrm{Load}}(t) \tag{9}$$

3.1.2. Battery

In this model, a simplistic battery model as proposed by Tremblay et al. [57] is adapted to the specific usecase. The main underlying model is the Shepherd model for constant-current discharge [58] with some modifications to consider the polarization voltage, known as modified Shepherd model [59]. Although more complex battery models, such as equivalent circuit models of first- and second order, can represent more accurate diffusion phenomena and voltage dynamics, the effect of these models does not affect the control approach proposed in this work [60]. The battery is modeled as a series controlled voltage source with constant resistance, as shown in Fig. 5. The model describes both charge and discharge behavior with similar characteristics.

The no-load voltage $E_{\mathrm{Bat}}(t)$ of the controlled voltage source can be described with the following relation:

$$E_{\mathrm{Bat}}(t) = E_{0,\mathrm{Bat}} - K \cdot \frac{Q_{\mathrm{nom}}}{Q_{\mathrm{nom}} - \int i_{\mathrm{Bat}}(t) \cdot dt} + A_{\mathrm{exp}} \cdot \exp(-B_{\mathrm{exp}} \int i_{\mathrm{Bat}}(t) \cdot dt), \tag{10}$$

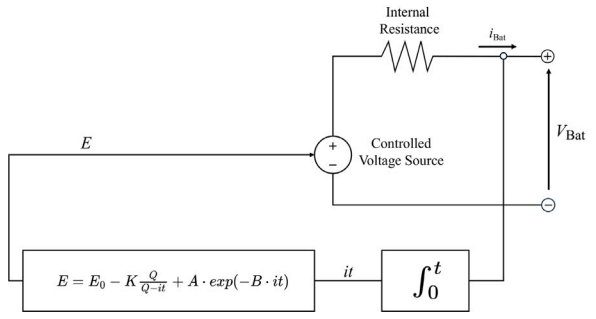

Fig. 5. Shepherd battery model [57].

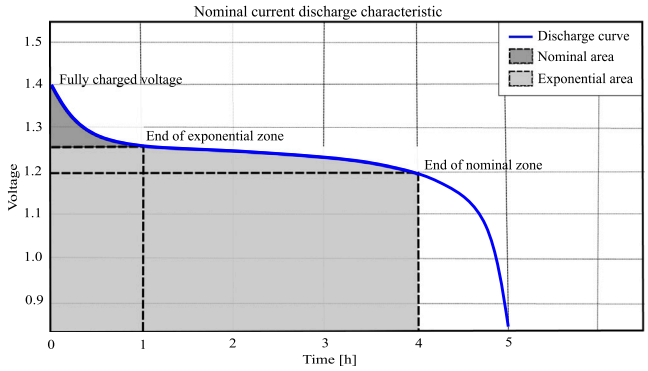

Fig. 6. Nominal current discharge characteristic for fitting of the battery model [57].

Table 4
Lithium-Ion battery parameters for a cell based on [57] and scaled model cells in parallel and series.

Parameter	Value	Unit
Q_{cell}	1	Ah
V_{cell}	3.6	V
E_0	3.7348	V
$R_{Bat,int}$	0.09	Ω
K	0.00876	V
A_{exp}	0.468	V
B_{exp}	3.5294	Ah^{-1}
n_p	2250	–
n_s	233	–

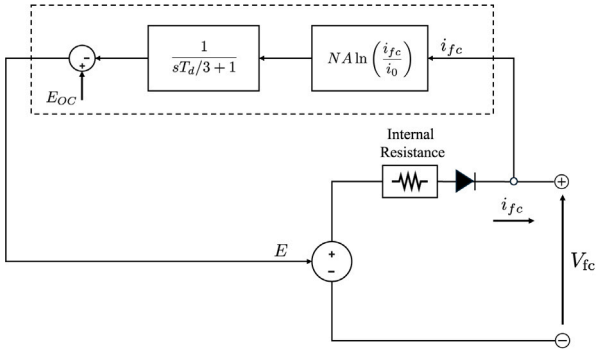

Fig. 7. Simplified fuel cell stack model [67].

where E_0 is the battery nominal voltage, K is the polarization voltage, Q_{nom} is the battery capacity, A_{exp} is the exponential zone amplitude, B_{exp} is the exponential zone time constant inverse, and $i_{Bat}(t)$ is the battery current over time. With this, the battery voltage V_{Bat} is defined as:

$$V_{Bat}(t) = E_{Bat}(t) - R_{Bat,int} \cdot i(t), \tag{11}$$

with the internal resistance $R_{Bat,int}$.

Following the Shepherd relation, the SOC of the battery can be considered inversely proportional to the polarization ohmic voltage and, therefore, be derived from this voltage-current approach [61]. As the SOC is a representation of how much capacity is left in the battery Q in comparison to the nominal capacity Q_{nom}

$$SOC(t) = \frac{Q(t)}{Q_{nom}} \cdot 100,$$

the model can be used to represent the SOC by estimating the battery voltage. This set of equations can be fitted for the parameters to fit the discharge curve of a battery. The resulting typical discharge curve is shown in Fig. 6.

A large benefit of this model is the capability to find the model parameters without experimental tests as they can be calculated using any typical discharge curve provided from a manufacturer sheet. Tremblay et al. [57] validate the approach for different battery chemistry discharge curves and derive the parameter sets for those respective batteries. Therefore, as reported in their work, the parameter set for a lithium-ion battery shown in Table 4 is used.

The model is based on the assumptions detailed in Tremblay et al. [57] and has two main limitations. The first is that the minimum no-load battery voltage is 0 V, while the maximum battery voltage is not limited. Second, the minimum capacity is limited to 0 A h, while the maximum capacity is not limited. From this, it follows that the SOC of the battery model can be greater than 100 % when overcharged. However, the control strategy limits the SOC of the battery to 80 % on the upper limit, which makes this limitation irrelevant for this application.

This battery model is scaled to fit the power system design shown in Table 2 and included in the virtual vessel simulation model. With the parameters for cell voltage V_{cell} and nominal cell capacity Q_{cell} the model is scaled by adjusting the number of cells in parallel and series to match the required nominal battery capacity Q_{Bat} and to match the DC system voltage. This leads to the numbers for cells in parallel n_p and cells in series n_s as shown in Table 4. In this, the battery model takes the battery current, determined by the power balance at the DC bus, and the initial value of the SOC for each time step as input. This battery current can be defined as follows for each of the two battery packs:

$$\dot{I}_{Bat,i}(t) = \frac{1}{2} \cdot \dot{I}_{Bat}(t).$$

Following the internal model, it provides the battery voltage V_{Bat} and an updated SOC as output, which are reported back to the energy system model.

3.1.3. Fuel cell

For the modeling of PEMFC, a variety of different modeling approaches are available in literature [62], such as different dynamic models [63–66] that can accommodate temperature or pressure changes. However, to integrate the model into a large marine energy system model, some simplifications can be made to speed up the simulation. In this application, the FC stack is simulated at nominal temperature and pressure conditions at all times, allowing for a simplified version of a stack model. In this work, the PEMFC is modeled according to Souleman et al. [67]. The authors propose a generic model that combines features from electrical and chemical models, which can be fitted by manufacturer data sheets. The simplified stack model consists of a series controlled voltage source with constant resistance, as shown in Fig. 7.

Similarly to the approach of the battery model, the controlled voltage source model aims to evaluate the FC voltage by determining the voltage of the controlled voltage source. The underlying base concept is

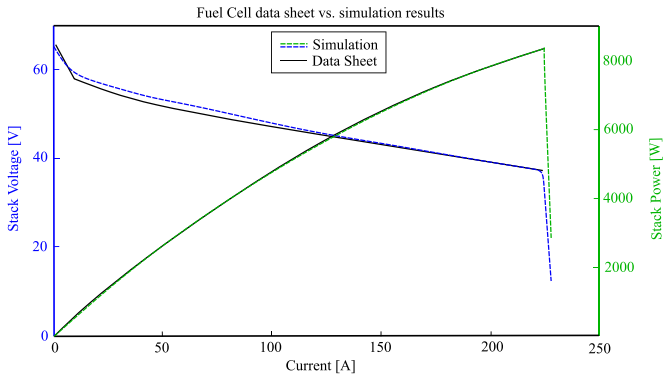

Fig. 8. Validation of the fuel cell stack model against a data sheet [67].

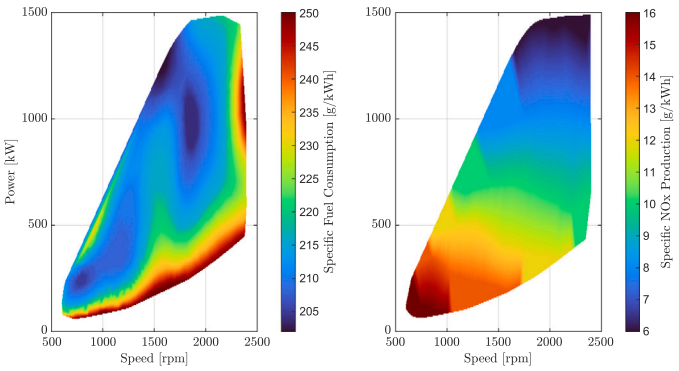

Fig. 9. SFC and NOx production maps of the ICE.

the Nernst equation [68], which is connected to both electrochemical and thermodynamic principles. The controlled voltage source can be described using the frequency domain as follows:

$$E_{\mathrm{FC}}(t) = E_{0,\mathrm{FC}} - N \cdot A \cdot \ln \frac{i(t)}{i_0} \cdot \frac{1}{s \cdot T_d/3 + 1}, \tag{12}$$

where $E_{0,\mathrm{FC}}$ is the open circuit voltage, N represents the number of cells in the stack, A is the Tafel slope, i_0 is the exchange current and T_d represents the response time. The current flowing in the fuel cell is represented by $i(t)$. This formulation considers only the activation losses, which occur due to the slowness of chemical reactions at the electrode's surface. Using this, the voltage of the fuel cell $V_{\mathrm{FC}}(t)$ can be determined, as follows

$$V_{\mathrm{FC}}(t) = E_{\mathrm{FC}}(t) - R_{\mathrm{FC,int}} \cdot i(t), \tag{13}$$

in which $R_{\mathrm{FC,int}}$ is the FC stack's internal resistance to include the ohmic losses.

The PEMFC model is controlled using a power reference $P_{\mathrm{FC,ref}}$, which is translated into a required current by

$$i(t) = \frac{P_{\mathrm{FC,ref}}(t)}{V_{\mathrm{FC}}(t)}. \tag{14}$$

With this, the hydrogen consumption of the FC is

$$m_{\mathrm{FC}}(t) = \frac{i(t) \cdot N}{z \cdot F} \cdot z = \frac{i(t) \cdot N}{F}, \tag{15}$$

where z is the number of moving electrons and F is the Farady constant [69].

The PEMFC selected for this study is the Nedstack FCS 13-XXL stack, with specifications derived from the manufacturer's technical data sheet [70]. At beginning-of-life, the stack delivers a rated electrical output of 13.6 kWe at a nominal current of 230 A. The system requires hydrogen fuel with a minimum purity of grade 2.5, compliant with ISO 14687-2:2008 standards. Operational requirements include a relative humidity of at least 50 % and a maximum hydrogen consumption of approximately 154 L min^{-1} (normalized). The manufacturer provides characteristic performance curves of stack voltage and output power as functions of the stack current, which were used to calibrate and validate the steady-state behavior of the model in this study [70]. Further information, such as temperature, emission production or inlet pressure are reported as well. Furthermore, experiments have been carried out to evaluate the behavior on other points of operation. The model performance shows an accurate representation of the real system for nominal conditions, as shown in Fig. 8.

3.1.4. Internal combustion engine

Modeling of ICE is a complex process involving several differential-equations, when trying to represent the dynamic thermodynamic behavior [71]. In recent years, a few approaches have been developed for ICE modeling. Approaches can be split into hybrid quasi-static models, single-zone thermodynamical models, and computational fluid dynamics (CFD) models [72]. While the first category of models is very fast but lacks in accuracy, the second and third categories can provide the required insights into fuel consumption and emission formation for the trade-off towards longer computational times. However, for the application in an energy management control framework, only the first category is feasible due to the prolonged computational times of the other approaches.

Therefore, maps created from experimental measurement data are used in this model. With this, the ICE are modeled using a simple map used for a look-up table and interpolation and real-world data measurements for the SFC and NO_x emission maps, shown in Fig. 9. This approach provides the results very fast and reliably and is considered accurate enough to show the proposed control application.

The used ICE model takes two values as inputs, both the engines speed $n_{\mathrm{Eng,i}}$ and the engines power $P_{\mathrm{Eng,i}}$. With this, the SFC, CO_2 and NO_x emissions are established. The data representing the SFC over the operational envelope is obtained from a map provided by the manufacturer for the Caterpillar C32, scaled to match the required operational power and speed of the engines used on the real vessel. The NO_x emission data is based on Geertsma et al. [11] and fitted to match the operational envelope of the SFC map. This approach is used as it is not common for engine manufacturers to provide complete maps of NO_x emissions. NO_x emissions are mainly driven by operating conditions and local combustion temperature, but limited data available. Therefore, obtaining NO_x emissions specific for the Caterpillar C32 was impossible. The representation used in this study shall illustrate the difference in the map for the SFC and NO_x emissions. However, as it aims to show the possibility of deciding between differently-natured objectives in this methodology, the map is suitable to demonstrate the approach.

3.1.5. Synchronous generator

This section presents the analytical approach to studying a synchronous generator's electrical behavior and main mechanical characteristics. Assuming a salient-pole machine and mechanical and electrical steady state, the machine's behavior has been studied according to [73,74]. The procedure is based on the analysis of the machine behavior along two axes, namely the direct axis d and the quadrature axis q, revolving with the rotor, according to the following relationship

$$\mathbf{E}_0 = \mathbf{V}_1 + R_a \mathbf{I}_a + jX_{sd}\mathbf{I}_{ad} + jX_{sq}\mathbf{I}_{aq}, \tag{16}$$

where X_{sd} and X_{sq} are the d-axis and q-axis synchronous reactance, respectively, $\mathbf{I}_{ad}$ and $\mathbf{I}_{aq}$ are the components of the armature current phasor along d-axis and q-axis respectively, $\mathbf{E}_0$ is the no-load phase voltage, $\mathbf{I}_a$ is the line current, $\mathbf{V}_1$ is the line phase voltage, X_s is the synchronous reactance, and R_a is the stator winding resistance (equivalent per phase).

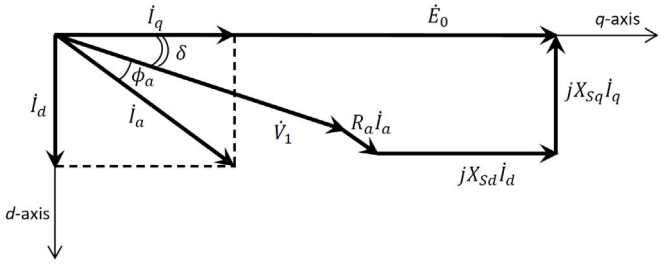

Fig. 10. Idealized salient-pole machine.

Eq. (16) can be easily translated into the phasor diagram reported in Fig. 10, where δ is the torque angle, representing the angle between the direct axis of the rotor and the direct axis of the stator, and ϕ_a represents the power angle, which is the phase angle difference between the armature current and the terminal voltage.

Thus, in the absence of saturation effects, the machine's behavior can be analyzed by solving Eq. (16), keeping in mind the linear relationship between the no-load voltage E_0 and the field current I_f. However, the analysis becomes more complex when saturation effects are present, as is commonly the case. Consequently, various methodologies to address this complexity have been developed and are well-documented in the literature [75]. In this application, the effects of saturation under load were considered using a saturation factor determined from the open-circuit characteristic.

To calculate the efficiency of a synchronous generator, the power components and system losses must be considered. The following equations express the relationships between the generated power components and the load requirements

$$P_1 = 3V_{1a}I_a\cos\phi_a = P_L + P_r \tag{17}$$

$$Q_1 = 3V_{1a}I_a\sin\phi_a = Q_L, \tag{18}$$

where P_1 is the active power produced by the synchronous generator, Q_1 is the reactive power produced by the synchronous generator, V_{1a} is the phase voltage of the generator, I_a is the armature current, ϕ_a is the power factor angle, P_L is the load power, P_r is the power loss in the rotor resistance, and Q_L is the reactive power consumed by the load.

The electromagnetic torque T_{em} is directly associated with the active power provided by the machine at the stator terminals. The relationship can be expressed as

$$T_{em} = \frac{P_1}{\omega_{c1}} = \frac{3V_{1a}I_a\cos\phi_a}{\omega_e} = \frac{P_L + P_r}{\omega_e}, \tag{19}$$

where ω_{c1} is the synchronous speed in mechanical radians per second and ω_e is the synchronous speed in electrical radians per second.

By expressing the power losses as frequency functions, the generator's efficiency can be derived as a function of frequency. P_r depends on the rotor resistance and the frequency, the friction and windage losses ($P_{\text{F\&W}}$) can be considered approximately constant, the core losses (P_{core}) typically increase with frequency due to hysteresis and eddy current losses, and joule losses (P_{J_s}) are dependent on the square of the current, which in turn is affected by frequency and load conditions. A loss analysis with a detailed examination and calculation of each loss component has been carried out to accurately estimate the efficiency of a synchronous generator.

When the generator operates under no-load conditions at synchronous speed, the mechanical power required represents the no-load rotational losses

$$P_{\text{no-load}} = P_{\text{F\&W}} + P_{\text{core}}, \tag{20}$$

where $P_{\text{no-load}}$ is the no-load power, $P_{\text{F\&W}}$ is the friction and windage loss, and P_{core} is the core loss. In the case of a short-circuit at synchronous speed, the losses due to armature current, P_{J_s}, known as short-circuit load loss, are given by:

$$P_{\text{short-circuit}} = P_{\text{F\&W}} + P_{J_s}, \tag{21}$$

where $P_{\text{short-circuit}}$ is the short-circuit power and P_{J_s} is the joule loss in the stator winding under short-circuit conditions. Since the DC resistance of the armature winding is known, the joule losses can be computed

$$P_{J_s} = 3R_aI_a^2, \tag{22}$$

Therefore, the overall shaft torque T_{shaft} and efficiency can then be calculated from the total mechanical power, factoring in all types of losses

$$T_{shaft} = \frac{P_{shaft}}{\omega_{c1}} = \frac{P_L + P_r + P_{\text{F\&W}} + P_{\text{core}} + P_{J_s}}{\omega_{c1}}, \tag{23}$$

where P_{shaft} is the total shaft power including all operational losses.

To calculate the efficiency of the synchronous generator η_{sg} as a function of frequency, the following equation is used

$$\eta_{sg} = \frac{P_{out}}{P_{in}} = \frac{P_L}{P_L + P_r + P_{\text{F\&W}} + P_{\text{core}} + P_{J_s}}, \tag{24}$$

where P_{out} is the useful power delivered to the load and P_{in} is the total input power including all losses. Using this model, an efficiency field for the generator can be created to showcase the different conversion efficiencies over the engine's operational envelope.

3.1.6. Energy conversion

The model contains several energy conversion components to integrate AC and DC into the system. Further, the mechanical losses at the gearbox are included similarly, as well as the losses of the electric motor. Those are modeled using linear efficiency factors as shown in Fig. 4.

3.1.7. Control inputs

The simulation model is controlled with eight reference set points. Four of them represent the ICE speeds and reference powers, while the other four are the FC power references. An interface is provided to either determine those set point values using a rule based controller or the ECMS controller, which is further outlined in the following.

3.2. Control development

The control development is split into a detailed description of the optimization problem and an analysis of its respective properties. Based on those, potential solution approaches and problems arising are discussed. Lastly, a hierarchical multi-level optimization is presented.

3.2.1. Optimization problem

States and controls can be defined to describe the system's mathematical behavior for the control problem. An overview of the state variables x_i, control variables u_i, inputs and parameters are presented in Tables 5 and 6. The five states are four time-dependent currents processed in the DC bus, namely the currents produced by the power sources, the battery current, the requested load current, and the SOC of the batteries. It is sufficient to consider one battery's SOC, as they are assumed to behave identically due to their direct connection to the bus. Those five states describe the actual system behavior depending on the choice of control variables u_i in the next time step. As control variables, the power and speed references for both ICE and the power set points for the FC are used.

As the system is continuous over time, all variables can be considered as time dependent functions. This leads to the following equation

Table 5
Control variables.

Name	Description	Role	
i_{Eng}	Engine Current	State (alg.)	x_1
i_{Load}	Requested Load Current	State (alg.)	x_2
i_{FC}	Fuel Cell Current	State (alg.)	x_3
i_{Bat}	Battery Current	State (alg.)	x_4
SOC_{Bat}	Battery State of Charge	State (dif.)	x_5
$P_{\text{Eng,i}}$	ith ICE Power Reference	Control	u_{1-2}
$n_{\text{Eng,i}}$	ith ICE Speed Reference	Control	u_{3-4}
$P_{\text{FC,j}}$	jth FC Power Reference	Control	u_{5-8}
P_{Prop}	Propulsion Load	Input	
P_{Aux}	Auxiliary Load	Input	
V_{DC}	DC Voltage	Input	
$V_{\text{FC,i}}$	Fuel Cell Voltage	Input	

Table 6
Control parameters.

Parameter	Description
N	Fuel Cell Cells in series
F	Faraday constant
p_{D}	Price of diesel
p_{H2}	Price of hydrogen
ζ_{Bat}	Equivalent factor battery
p_{Bat}	Equivalent price battery
n_{p}	Battery modules in parallel
Q_{nom}	Battery nominal power
η_{gb}	Gearbox loss
η_{m}	Electric motor loss
$\eta_{\text{AC-DC}}$	AC-DC conversion loss
$\eta_{\text{DC-AC}}$	DC-AC conversion loss
$\eta_{\text{DC-DC}}$	DC-DC conversion loss

system for the system behavior represented by the state variables:

$$\begin{aligned}
x_1(t) &= \frac{u_1(t)\cdot\eta_{Gen,1}(t)+u_2(t)\cdot\eta_{Gen,2}(t)}{V_{\text{DC}}(t)}\cdot\eta_{\text{AC-DC}}\\
x_2(t) &= \frac{P_{\text{Prop}}(t)\cdot 1/\eta_{gb}\cdot 1/\eta_m + P_{\text{Aux}}(t)}{V_{\text{DC}}(t)\cdot\eta_{\text{DC-AC}}}\\
x_3(t) &= \frac{(u_5(t)+u_6(t)+u_7(t)+u_8(t))}{V_{\text{DC}}(t)}\cdot\eta_{\text{DC-DC}}\\
x_4(t) &= x_1(t)+x_3(t)-x_2(t)\\
x_5(t) &= x_5(0)+\frac{1}{2}\int_0^t \frac{x_4(t)}{Q_{\text{nom}}\cdot n_p}\,dt
\end{aligned} \tag{25}$$

However, solving a continuous time control problem can be challenging computationally. Discretizing the system with an appropriate sampling rate solves this problem while still providing an accurate representation of the system behavior, wherefore the behavior in between the sample points can be neglected [76]. This leads to the discretized variable system of a time step n reported in Eq. (26). In this, Δt is the sampling rate between the time steps k.

$$\begin{aligned}
x_1 &= \frac{u_1\cdot\eta_{Gen,1}+u_2\cdot\eta_{Gen,2}}{V_{\text{DC}}}\cdot\eta_{\text{AC-DC}}\\
x_2 &= \frac{P_{\text{Prop}}\cdot 1/\eta_{gb}\cdot 1/\eta_m + P_{\text{Aux}}}{V_{\text{DC}}\cdot\eta_{\text{DC-AC}}}\\
x_3 &= \frac{(u_5+u_6+u_7+u_8)}{V_{\text{DC}}}\cdot\eta_{\text{DC-DC}}\\
x_4 &= x_1+x_3-x_2\\
x_5 &= x_{5_{k-1}}+\frac{1}{2}\frac{\Delta t\cdot x_4}{Q_{\text{nom}}\cdot n_p}
\end{aligned} \tag{26}$$

While most efficiencies in Eq. (26) are constant quantities and handled as parameters of the problem, the transformation of the mechanical power of the engines into electric current is handled differently. Synchronous generators are used for the transformation of mechanical into electrical energy. As the conversion efficiency is not constant, a field is used to account for the variable speed operation and the switching efficiencies. In the controller, this variable efficiency is also represented by a function f_1 in the form of

$$\eta_{\text{Gen}} = f_1(u_i, u_{i+2}), \tag{27}$$

which is also depending on the speed and power produced by the engines $i \in \{1,2\}$.

Fuel consumption and emission production. To further quantify the system behavior by adding objectives, an additional set of functions can be defined to describe the fuel consumption and emission production under operation. For this, first, the combination of power and speed control values of the ICE to the SFC and NO_x emissions are related. Mathematically, the fuel consumption and the NO_x emissions are represented as rates Θ to evaluate the production over time. The rates $\Theta_{\text{SFC,Eng}}$ and $\Theta_{\text{NO}_x\text{,Eng}}$ can be defined using the fuel maps of the ICE, shown in Fig. 9. Mathematically, two additional functions f_2 and f_3 for the ICE indexed with $i \in \{1,2\}$ are defined in the following form:

$$\Theta_{\text{SFC,Eng,i}} = f_2(u_i, u_{i+2}) \tag{28}$$

$$\Theta_{\text{NO}_x\text{,Eng,i}} = f_3(u_i, u_{i+2}), \tag{29}$$

in which the functions represent the SFC and NO_x production rates. Using those, the consumed mass of diesel fuel m_{D} and the NO_x emissions produced m_{NO_x} can be determined as follows:

$$m_{\text{D}} = \Theta_{\text{SFC,Eng,1}}\cdot u_1 + \Theta_{\text{SFC,Eng,2}}\cdot u_2 \tag{30}$$

$$m_{\text{NOx}} = \Theta_{\text{NO}_x\text{,Eng,1}}\cdot u_1 + \Theta_{\text{NO}_x\text{,Eng,2}}\cdot u_2 \tag{31}$$

In addition, the consumed mass of hydrogen fuel (m_{H2}) from the FCs can be established using the following relation:

$$m_{\text{H2}} = \left(\sum_{i=1}^{4}\frac{u_{4+i}}{V_{\text{FC},i}}\right)\cdot\frac{N}{F}, \tag{32}$$

where N represents the number of cells in series within the fuel cell stack, $V_{\text{FC,i}}$ denotes the voltage of the ith fuel cell, and F is the Faraday constant. With this, the fuel mass consumed and emission produced for both hydrogen and diesel can be estimated in relation to the control power set points.

Battery equivalent factor. The key element of ECMS is the use of equivalence factors to allow for the comparison of differently natured energy sources. In this case, a battery equivalent factor ζ is introduced to compare the electric energy to the chemical energy in the two fuels diesel and hydrogen. This battery factor is designed to determine the optimal power split for an optimal operation of all three power sources sidealong. While previous work often uses a constant value for the equivalence factor [28,46], this study proposes an adaptive factor to improve the holistic optimization of the power split.

First, the battery power is computed based on the battery current x_4 to compare the battery with the other power sources, which are controlled by power set points, in the following way

$$P_{\text{Bat}} = |x_4|\cdot V_{\text{DC}}. \tag{33}$$

Now, the battery power P_{Bat} is relatable to the powers of the other energy sources. As the dynamics of the ICEs and batteries are faster than the FCs, those two components are intended to deal with the variations of the load profile, while the FCs are best operated on constant load without fast changes. As the SFC of the engine is highly nonlinear over the operational envelope, compare Fig. 9, the battery can be used to optimize the point of engine operation. For this, the battery power is transformed into virtual diesel fuel mass using the adaptive equivalent factor.

Therefore, three cases of operation are defined, for which each an equivalent factor is designed: (1) battery + FC only operation, (2) battery + FC + 1 ICE operation, and, (3) battery + FC + 2 ICE operation.

The most simple is case (1), in which a constant factor ζ_1 is chosen, as no engine is running:

$$\zeta_1 = \min(\Theta_{\mathrm{SFC,Eng}}), \tag{34}$$

which is the point of minimal engine fuel consumption. For case (2) and case (3), the equivalent factors ζ_2 and ζ_3 are online adaptive to the actual SFC of the ICE. This is done as follows for case (2):

$$\zeta_2 = \Theta_{\mathrm{SFC,Eng,1}}, \tag{35}$$

and case (3):

$$\zeta_3 = \frac{\Theta_{\mathrm{SFC,Eng,1}} + \Theta_{\mathrm{SFC,Eng,2}}}{2}. \tag{36}$$

With this factor ζ_i with $i \in \{1,2,3\}$, the equivalent virtual fuel mass consumed by the battery m_{Bat} can be described using the power P_{Bat} following

$$m_{\mathrm{Bat}} = \zeta_i \cdot P_{\mathrm{Bat}}, \tag{37}$$

depending on the case of operation.

Objective function. Next, the objective function of the optimization problem can be set up. The objective function defines a direction toward the optimal solution of the control problem by defining targets to minimize over the course of the operation. The objectives considered in this study are the minimization of both fuels consumed, as well as NO_x emissions. The two fuels, hydrogen and diesel, are each related to a financial cost p_{D} and pH2 to quantify the cost of consumption. With the virtual battery fuel mass m_{Bat} calculated in Eq. (37) the battery power is transformed to diesel equivalent by using the equivalent factor ζ and can be examined with the price for diesel as well.

Two objectives C_i with $i \in \{1,2\}$ are defined in the form of

$$C_1 = m_{\mathrm{D}} \cdot p_{\mathrm{D}} + m_{\mathrm{H2}} \cdot p_{\mathrm{H2}} + m_{\mathrm{Bat}} \cdot p_{\mathrm{D}} \tag{38}$$

$$C_2 = m_{\mathrm{NOx}}, \tag{39}$$

where C_1 represents the financial cost and C_2 the produced emissions. Both aspects are normalized to allow for a comparison of the differently natured objectives. In addition, a weight λ is introduced to allow the operator to prioritize between the objective of financial cost minimization and emission production. This leads to the following objective function formulation

$$J(\mathbf{x},\mathbf{u}) = \lambda \cdot C_1 + (1-\lambda) \cdot C_2 \tag{40}$$

Constraint definition. A set of equality and inequality constraints further defines the system's behavior. The most important equality constraint used is the power balance. This constraint ensures that the amount of generated power matches the required power and is critical to ensure the stability of the electric system. The power balance is reported in Eq. (41).

$$0 = x_1 + x_3 - x_2 - x_4 \tag{41}$$

For each component, a set of inequality constraints describes the operational envelope introducing a lower and upper limit. For a generic component $\mathcal{O}$, those constraints can be represented in the form of

$$\mathcal{O}_{\mathrm{lower}} \le \mathcal{O} \le \mathcal{O}_{\mathrm{upper}}. \tag{42}$$

However, the engines cannot be described in this form, as they need to be represented by an operational envelope diagram, as shown in Fig. 9. Two functions dependent on the engine power and engine speed are introduced to define the upper and lower limits of the characteristics map. This leads to the functions reported in Eq. (43) for engines $i \in \{1,2\}$.

$$f_{\mathrm{lower,i}}(u_{\mathrm{i,lower}}, u_{\mathrm{i+2,lower}}) \le \mathcal{O}_{\mathrm{Eng,i}} \le f_{\mathrm{upper,i}}(u_{\mathrm{i,upper}}, u_{\mathrm{i+2,upper}}) \tag{43}$$

Those functions alone are not enough to fully describe the operation of the ICEs. A relevant aspect of the engine operation is the possibility of it not operating, introducing a mixed-integer aspect to the problem. The engine speed can be defined in the following interval $n \epsilon N = \{0, u_{\mathrm{i+2,lower}} \le u_{\mathrm{i+2}} \le u_{\mathrm{i+2,upper}}\}$. Using this, the power of the engines $i \in \{1,2\}$ is constrained as follows:

$$u_{\mathrm{i}} \le \delta_{u_{\mathrm{i+2}}} \cdot f_{\mathrm{upper,i}}(u_{\mathrm{i}}, u_{\mathrm{i+2}}) \tag{44}$$

$$u_{\mathrm{i}} \ge \delta_{u_{\mathrm{i+2}}} \cdot f_{\mathrm{lower,i}}(u_{\mathrm{i}}, u_{\mathrm{i+2}}) \tag{45}$$

using the Kronecker delta $\delta_{u_{\mathrm{i+2}}}$ defined as follows:

$$\delta_{u_{\mathrm{i+2}}} = \begin{cases} 1, & \text{if } u_{\mathrm{i+2,lower}} \le u_{\mathrm{i+2}} \le u_{\mathrm{i+2,upper}}, \\ 0, & \text{else.} \end{cases} \tag{46}$$

Similarly, the battery is also defined by additional constraints. As mentioned above, the batteries have two characteristic variables, the current coming from or going towards the batteries and the SOC. Since the batteries are doubled and directly connected to the bus, each battery pack is considered to be receiving/providing half of the current in the current time step (See Eq. (47)).

$$I_{\mathrm{Bat,1}} = \frac{1}{2} \cdot x_4 = I_{\mathrm{Bat,2}} \tag{47}$$

This leads to both batteries always having the same SOC, which is a simplification of reality, but for this purpose, it is accurate enough. An additional inequality constraint limits the absolute change in SOC, which is represented as change Δx_5 over the course of one time step k, as follows

$$0 \le |\Delta x_5| = |x_{5,k+1} - x_{5,k}| \le \Delta x_{5_{\max}}. \tag{48}$$

While upper and lower limits are introduced for both the SOC, the change of the SOC over time and the battery current, as well as the choice of battery mode, require further consideration. A battery mode is used to actively manage the long-term trend of the batteries actively, even though the batteries are indirectly controlled using the power generation by the ICEs and FCs. Two modes are considered for the battery: charging and discharging, meaning that over the operational time the aim is to either charge or discharge the batteries. This adds another mixed-integer aspect to the complexity of the problem. Coherent to the choice of battery mode, additional constraints can be defined for the battery operation. If the battery is in discharging mode, the following constraint applies

$$\Delta x_5 - \Delta x_{5_{\max}} \le 0, \tag{49}$$

which ensures that the battery is discharged. On the contrary, in charging mode, the constraint is defined as follows

$$\Delta x_{5_{\min}} - \Delta x_5 \le 0, \tag{50}$$

where $\Delta x_{5_{\min}}$ is the minimum change in SOC over the time step to ensure the battery is slowly charged. The battery mode should be switched when the SOC approaches the upper or lower limit, respectively.

Complete formulation. This mathematical construct allows to formulate the optimization problem as reported in Eq. (51)

$$\begin{aligned} &\text{Minimize:} \quad J(\mathbf{u}(\cdot|k)) \\ &\quad \text{s.t.:} \\ &\qquad \mathbf{x}_{k+1} = f(\mathbf{x}_k, \mathbf{u}_k) \\ &\qquad \mathbf{u}_k = \mathbf{u}_{k-1} + \Delta\mathbf{u}_k \\ &\qquad g_{\mathrm{in}}(\mathbf{x}_k, \mathbf{u}_k) \le 0 \\ &\qquad g_{\mathrm{eq}}(\mathbf{x}_k, \mathbf{u}_k) = 0, \end{aligned} \tag{51}$$

where $\mathbf{x}_{k+1}$ represents the state at the next time-step as a function of the current state, $\mathbf{x}_k$, and the current control, $\mathbf{u}_k$, which is the evolution of the control input derived by adjusting the control from the preceding time-step, $\mathbf{u}_{k-1}$, by an increment, $\Delta\mathbf{u}_k$. g_{in} and g_{eq} represent the set of

inequality and equality constraints of the problem. This results in the complete optimization problem, as follows:

$$
\begin{aligned}
\text{Minimize:}\quad & J(\mathbf{x},\mathbf{u}) = \lambda \cdot C_1 + (1-\lambda)\cdot C_2 \\
\text{s.t.:}\quad & \\
& \mathbf{x}_{1,k+1} = \frac{\mathbf{u}_{1,k}\cdot\eta_{Gen,1,k} + \mathbf{u}_{2,k}\cdot\eta_{Gen,2,k}}{V_{\mathrm{DC}}}\cdot\eta_{\mathrm{AC-DC}} \\
& \mathbf{x}_{2,k+1} = \frac{P_{\mathrm{Prop}}\cdot 1/\eta_{gb}\cdot 1/\eta_m + P_{\mathrm{Aux}}}{V_{\mathrm{DC}}\cdot\eta_{\mathrm{DC-AC}}} \\
& \mathbf{x}_{3,k+1} = \frac{(\mathbf{u}_{5,k}+\mathbf{u}_{6,k}+\mathbf{u}_{7,k}+\mathbf{u}_{8,k})}{V_{\mathrm{DC}}}\cdot\eta_{\mathrm{DC-DC}} \\
& \mathbf{x}_{4,k+1} = \mathbf{x}_{1,k+1} + \mathbf{x}_{3,k+1} - \mathbf{x}_{2,k+1} \\
& \mathbf{x}_{5,k+1} = \mathbf{x}_{5,k} + \frac{1}{2}\frac{\Delta t\cdot\mathbf{x}_{4,k+1}}{Q_{\mathrm{nom}}\cdot n_p} \\
& \mathbf{u}_{1,k} = \mathbf{u}_{1,k-1} + \Delta\mathbf{u}_1 \\
& \mathbf{u}_{2,k} = \mathbf{u}_{2,k-1} + \Delta\mathbf{u}_2 \\
& \mathbf{u}_{3,k} = \mathbf{u}_{3,k-1} + \Delta\mathbf{u}_3 \\
& \mathbf{u}_{4,k} = \mathbf{u}_{4,k-1} + \Delta\mathbf{u}_4 \\
& \mathbf{u}_{5,k} = \mathbf{u}_{5,k-1} + \Delta\mathbf{u}_5 \\
& \mathbf{u}_{6,k} = \mathbf{u}_{6,k-1} + \Delta\mathbf{u}_6 \\
& \mathbf{u}_{7,k} = \mathbf{u}_{7,k-1} + \Delta\mathbf{u}_7 \\
& \mathbf{u}_{8,k} = \mathbf{u}_{8,k-1} + \Delta\mathbf{u}_8 \\
g_{\mathrm{in}} = {} & \mathcal{O}_{\mathrm{lower}} - \mathcal{O} \\
& \mathcal{O} - \mathcal{O}_{\mathrm{upper}} \\
& f_{\mathrm{lower},1}(\mathbf{u}_{1,k},\mathbf{u}_{3,k}) - \mathcal{O}_{\mathrm{Eng},1} \\
& f_{\mathrm{lower},2}(\mathbf{u}_{2,k},\mathbf{u}_{4,k}) - \mathcal{O}_{\mathrm{Eng},2} \\
& \mathcal{O}_{\mathrm{Eng},1} - f_{\mathrm{upper},1}(\mathbf{u}_{1,k},\mathbf{u}_{3,k}) \\
& \mathcal{O}_{\mathrm{Eng},2} - f_{\mathrm{upper},2}(\mathbf{u}_{2,k},\mathbf{u}_{4,k}) \\
& -|\Delta\mathbf{x}_5| \\
& |\Delta\mathbf{x}_5| - \Delta\mathbf{x}_{5\max} \\
& \Delta\mathbf{x}_5 - \Delta\mathbf{x}_{5\max} \\
& \Delta\mathbf{x}_{5\min} - \Delta\mathbf{x}_5 \\
& \mathbf{u}_1 - \delta_{u_3}\cdot f_{\mathrm{upper},1}(\mathbf{u}_1,\mathbf{u}_3) \\
& \mathbf{u}_3 - \delta_{u_4}\cdot f_{\mathrm{upper},2}(\mathbf{u}_3,\mathbf{u}_4) \\
& \delta_{u_1}\cdot f_{\mathrm{lower},1}(\mathbf{u}_1,\mathbf{u}_3) - \mathbf{u}_1 \\
& \delta_{u_2}\cdot f_{\mathrm{lower},2}(\mathbf{u}_2,\mathbf{u}_4) - \mathbf{u}_2 \\
g_{\mathrm{eq}} = {} & \mathbf{x}_{1,k+1} + \mathbf{x}_{3,k+1} - \mathbf{x}_{2,k+1} - \mathbf{x}_{4,k+1} \\
& \eta_{\mathrm{Gen},1,k} - f_1(\mathbf{u}_{1,k},\mathbf{u}_{3,k}) \\
& \eta_{\mathrm{Gen},2,k} - f_1(\mathbf{u}_{2,k},\mathbf{u}_{4,k}) \\
& \Theta_{\mathrm{SFC,Eng},1} - f_2(\mathbf{u}_{1,k},\mathbf{u}_{3,k}) \\
& \Theta_{\mathrm{SFC,Eng},2} - f_2(\mathbf{u}_{2,k},\mathbf{u}_{4,k}) \\
& \Theta_{\mathrm{NO}_x,\mathrm{Eng},1} - f_3(\mathbf{u}_{1,k},\mathbf{u}_{3,k}) \\
& \Theta_{\mathrm{NO}_x,\mathrm{Eng},2} - f_3(\mathbf{u}_{2,k},\mathbf{u}_{4,k}),
\end{aligned}
\tag{52}
$$

where $\mathcal{O}$ represents the different components of the system besides the engines.

3.2.2. Problem analysis and solution approach

An analysis of the problem is required to determine an adequate solution approach. Two aspects require special focus in the set up of the optimization problem. First, the ICEs can be either on or off, leading to a mixed-integer (MI) decision. Second, the ICEs SFC and NOx functions have a non-linear (NL) nature. With this analysis, the optimization problem can be defined as a MINL programming problem [77]. Moreover, taking into account that not all functions of the problem are convex, the problem becomes non-convex as well [78,79], and therefore computationally difficult to solve [80].

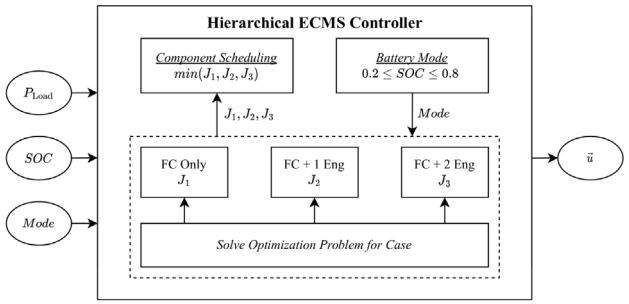

Fig. 11. Overview of the hierarchical control approach.

The problem can be split into different steps to address those difficulties and combine them in a hierarchical controller. Fig. 11 shows the proposed hierarchical ECMS control structure. The problem is divided into the mixed-integer component scheduling and battery mode selection and the non-linear optimization of the component's operating points. The battery mode is selected based on the momentary SOC and the mode the battery is in initially. This is done to ensure a continuous charging or discharging operation over time and to change the mode when the respective limit is reached. Based on the battery's mode, the optimization problem considers different constraints. The optimization problem is solved for three cases: An operation just using FCs, using the FCs combined with one engine and using the FCs and two engines. This is also highlighted in the choice of battery equivalent factor in the optimization problem. The objective function values J_i for the cases $i \in \{1,2,3\}$ are handed over to the component scheduling layer, which selects the case with the minimum objective function value. The component scheduling layer then sets the optimized control values for the operating components while the rest is set to zero. The algorithm's structure is also shown in Alg. 1. Furthermore, to avoid constant jumping of the control values between the time steps, a buffer is implemented. If the change in load request ΔP_{Load} is smaller than an assigned value for allowed fluctuation $\Delta P_{\mathrm{Fluctuation}}$ and the battery mode requires no change, then the previous set points are kept for the upcoming time step as well. This way, even though the problem needs to be solved three times instead of just once, the solution time improves greatly in comparison to the MINLP solution time, as the complexity of the problem itself is reduced drastically.

This solves the problems caused by the mixed-integer nature. However, the optimization itself has to find a global minimum in a non-convex problem, which requires global optimization approaches. Global optimization approaches, such as genetic algorithms, are well-known to be very slow. As real-time optimization potential is also a relevant criterion for the application, local optimization algorithms are considered as well. While local optimization does not guarantee finding the global minimum of a problem, it can be combined with a multi-start approach. This way, the optimization started multiple times from different starting points and the results are compared to single out the global minimum. If local optimizers manage to achieve a solution in a faster time than global optimization without too many iterations, it is a feasible solution to achieve real-time control. Therefore, three local optimizers (interior-point (IP) [81], active set (AS), sequential quadratic programming (SQP) [82]), as well as a gradient free method (Pattern Search (PS)), all implemented using a multi-start approach are compared with a global optimization approaches (Genetic Algorithm (GA)).

4. Simulation study

For evaluation of the proposed ECMS control approach, an example load profile based on Fig. 1 is chosen and tested with the simulation model. For this study, a few parameters are used to evaluate the

Algorithm 1 Hierarchical ECMS Control Algorithm

Require: ΔP_{Load}, SOC, Mode
  if SoC ≤ 0.2 **then**
    Mode $= 0$ ▷ *Battery mode charge*
  else if SoC ≥ 0.8 **then**
    Mode $= 1$ ▷ *Battery mode discharge*
  else if $\Delta P_{\text{Load}} \leq \Delta P_{\text{Fluctuation}}$ **then**
    $P_{\text{Set}} = P_{\text{Set,i-1}}$ ▷ *Keep old setpoints*
  end if
  ▷ *Run optimization for all three configurations.* ◁
  function RUNCONTROLLERS(P_{Load}, SOC, Mode)
    $J_1, P_{\text{Set},1}$ ▷ *Optimize configuration 1*
    $J_2, P_{\text{Set},2}$ ▷ *Optimize configuration 2*
    $J_3, P_{\text{Set},3}$ ▷ *Optimize configuration 3*
  end function
  ▷ *Evaluate objective function value for all configurations and chose new setpoints.* ◁
  if $min\{J_1, J_2, J_3\} = J_1$ **then**
    $P_{\text{Set}} = P_{\text{Set},1}$
  else if $min\{J_1, J_2, J_3\} = J_2$ **then**
    $P_{\text{Set}} = P_{\text{Set},2}$
  else if $min\{J_1, J_2, J_3\} = J_3$ **then**
    $P_{\text{Set}} = P_{\text{Set},3}$
  end if

Table 7
Parameters used for evaluation.

Parameter	Description	Value
ρ_D	Density diesel	0.838 kg/l
r_{CO2}	CO2 release rate	2.7 t CO2/l
p_D	price diesel	0.7 e /l
p_{H2}	price hydrogen	9.4 e /kg
p_{NOx}	price NOx	2.26 e /kg
p_{CO2}	price CO2	0.09 e /kg

performance of the control operation shown in Table 7. The economic costs are based on current market prices for hydrogen and diesel. To quantify the impact of NO_x emissions and the CO_2 release in terms of economic aspects, an estimate of how a potential price could be attributed to emissions in €/kg in the future is used. This is orientated on a report analyzing scenarios about NO_x controls for shipping in EU seas [83] and a sensitivity analysis.

4.1. Load profile

For the study, an example load profile of 120 h is chosen, containing both propulsion and auxiliary demand. Fig. 12 shows the propulsion load in blue, the auxiliary load demand in red and the combined total load in black. The load profile chosen is exemplary for a variety of different tasks performed by the vessel. At the beginning and the end, the vessel only uses auxiliary load, so it is stationary in port or at anchor. At around 20 h, low propulsion power is occurring which can represent manoeuvring or low speed sailing operation, most probably inside a port or in an inland water way. Afterwards, high propulsion loads are requested, representing sailing at different speeds with a short interruption. This interruption can be related to either lower speed sailing while being in a restricted area or a dynamic positioning operation in front of the coast. Afterwards, sailing is resumed and the port is reached again, when the electric power request returns to auxiliary load only. This load profile is chosen to show the performance of the proposed controller in dealing with the various operations and the fast changes in between.

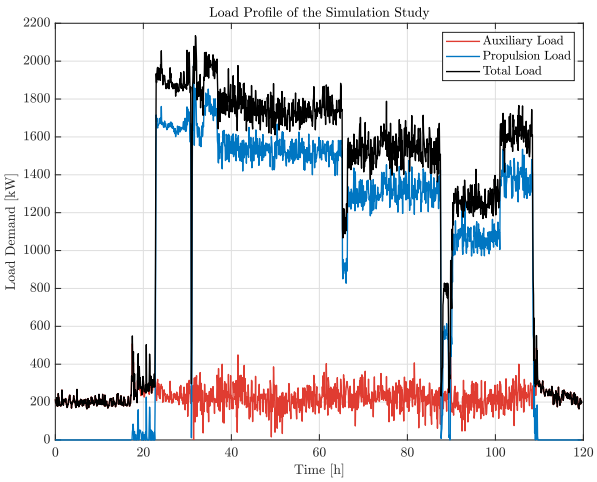

Fig. 12. Load profile of 120 h used in the simulation study.

4.2. Benchmark

As benchmark for this study, two cases are considered and tested. The first is the common industry diesel-electric vessel layout featuring four diesel generators in an AC shipboard power grid. The engines are operated with a simple RBC to do efficient tracking of the requested power. This benchmark will be referred to as B1 (benchmark 1) in the discussion. The second reference benchmark will be the retrofitted vessel operated with RBC and be referred to as B2 (benchmark 2). The RBC algorithm for the retrofitted vessel is already a more advanced version that accommodates the power split between FC, ICE and batteries to reduce the fuel consumption.

Rule-based control retrofit. The rule-based controller to operate the retrofitted vessel is developed to determine the powersplit between the three component types with a single-objective. This objective is reducing fuel consumption from an economic perspective, which relates the costs of diesel with the cost of hydrogen. Taking this into account, the control philosophy of the controller is to allow the power generation components in point of high efficiency and using the battery to buffer for the fluctuation of the power demand from the most optimal points. This means, it tries to operate the FC at low loads, where they are most efficient and the ICE in points of low SFC, referring to Fig. 9. Further a battery mode is integrated to maintain a steady charge or discharge trend, similar to the ECMS controller. A schematic of the rule-based (RB) controller is shown in Fig. 13. This is also depicted as an algorithm in Alg. 2.

The controller is developed to follow large changes in the load using the engines while maintaining the FCs at efficient low load setpoints. Moreover, the battery is used to buffer small changes in the load request. This means that if the change in requested load $P_{\text{Load}} - P_{\text{Load,n-1}}$ is smaller than 150 kW and the battery is not below the lower or above the upper limit, previous setpoints are maintained. To maintain a steady charging or discharging operation, the exact setpoints for the engine are based on the battery mode. If the battery is in discharging mode, the setpoint will be chosen smaller than the actual load demand, while the set point is chosen to be higher than the load in charging mode.

The RBC controller is tested on the load profile to establish a benchmark. The discretization time step size is chosen to be similar to the step size of the ECMS controller to allow a fair comparison. The load balance, the corresponding battery SOC, and the DC system voltage are shown in Fig. 14. The RBC manages to maintain the power balance while slowly charging and discharging the battery over the course of the operation. It can be observed that the FCs are mainly maintained at a low load, which is beneficial for both the economical aspect as well as the degradation of the fuel cell by avoiding high loads.

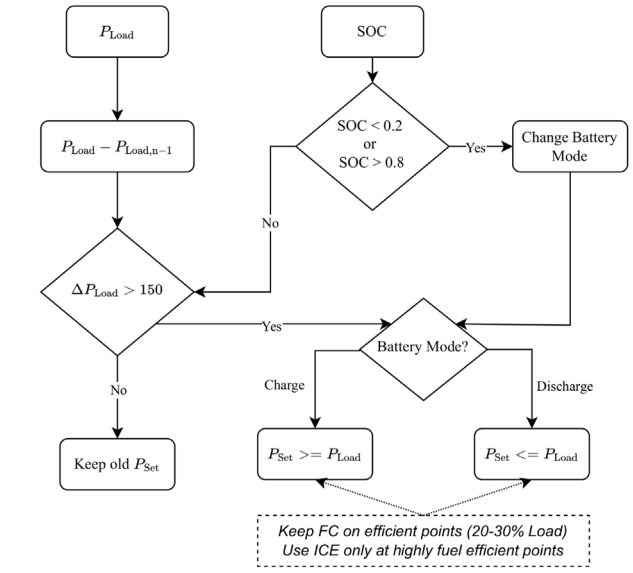

Fig. 13. Schematic of the rule-based controller of the retrofitted vessel used as benchmark.

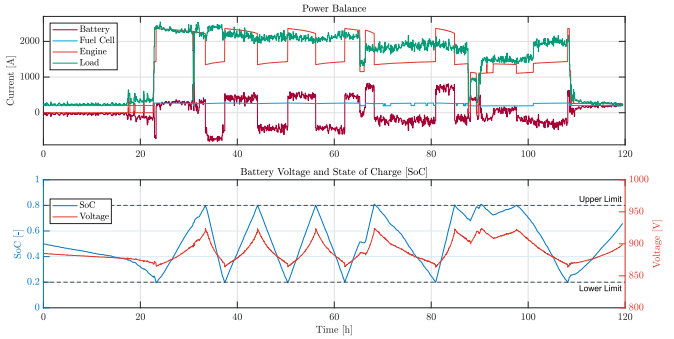

Fig. 14. Power balance, battery SoC and DC system voltage operating the system with the rule-based controller.

4.3. Solution algorithm

Preliminary to the simulation study with the ECMS controller on the complete load profile, an investigation of solution approaches is carried out. A solution algorithm for the complete study based on the actual performance and the time required to find a feasible solution can be selected. All algorithms are tested on the exact same point of the load profile starting from a similar state. The chosen point has a required load demand of $P_{Load} = 1885kW$ and is investigated with both controllers, one engine only and two engines. Further, the objective function weights are also pre-defined to examine all solution algorithms on exactly the same problem. All algorithms are also tested with similar error tolerance for the objective function and constraints. The criteria for a comparison are the value of the objective function J, the iterations required for a solution, the function count and the step-size for the local optimizers, as well as the mesh-size of the pattern search and the generations of the genetic algorithm. The GA is evaluated with a population size of 50. Furthermore, the time to find this solution is compared as well. An overview of the comparison is shown in Table 8. The comparison shows that all algorithms minimize the function to a relatively similar value, with changes only on the second or third decimal place. However, the solution times differ greatly. It can be distinguished that SQP offers a very good minimization compared to the others while also being faster in solution time. Therefore, the ECMS controller study is conducted using a SQP multi-start approach.

Algorithm 2 Rule-Based Control Algorithm

```
if SOC ≤ 0.2 then
    Mode_B = 0                                   ▷ Battery mode charge
else if SOC ≥ 0.8 then
    Mode_B = 1                                   ▷ Battery mode discharge
end if
Require: ΔP_Load = |P_Load,i − P_Load,i−1|
if ΔP_Load ≥ 150 then                            ▷ Check load fluctuation
    if Mode_B = 0 then
        P_Set ≥ P_Load
    else if Mode_B = 1 then
        P_Set ≤ P_Load
    end if
else
    P_Set = P_Set,i−1                            ▷ Keep old setpoints
end if
```

Table 8
Comparison of solution algorithms.

Criteria	SQP	IP	AS	PS	GA
	1 Engine and 4 Fuel Cells				
Cost Function	0.3558	0.3560	0.3806	0.3894	0.3592
Solution Time	6.94	11.62	16.02	13.7	93.22
Iterations	19	17	2	3	
Generations					7
Function Count	230	171	14	549	31432
Mesh-size				1e-07	
	2 Engine and 4 Fuel Cells				
Cost Function	0.1545	0.1613	0.1582	0.1522	0.1592
Solution Time	6.33	8.53	12.68	58.14	124.32
Iterations	38	85	2	3	
Generations					5
Function Count	399	1065	18	15673	33309
Mesh-size				1e-07	

4.4. ECMS control

The performance of the ECMS controller is tested in three different scenarios. First, the ECMS powersplit with a single focus on SFC consumption (SFC-Only) is tested, where the objective weights are fixed on [1 0]. Subsequently, the performance of the multi-objective control version is investigated, employing a Pareto frontier for the selection of the solution. As the computation of a full Pareto frontier is computationally expensive, the scenario of using a full Pareto frontier (F-P) is compared to a reduced version, which accounts for a pre-selected bias based on a mode to investigate areas of the Pareto frontier (MB-P). This is done to investigate what influence the preliminary bias introduces and if the computational time can be reduced by the mode based operation without missing out on performance.

For the reduced Pareto frontier, a mode is introduced based on a simple principle. It separates between periods with mainly auxiliary load and periods with propulsion loads due to the following: Zero or low propulsion load in the load profile resembles a mode in which the yacht is either on anchor or in the harbour, for which a low emission output is considered as very beneficial. Therefore the Pareto frontier investigates 10%–40% focus on fuel consumption and the respective 60%–90% focus on NOx emission. When the yacht is sailing, resembled by a high propulsion load, the opposite Pareto frontier is used, as reduction of fuel consumption is beneficial for the economic aspect as well as the autonomous travel distance, while potential rules for emission production, which may be in place at anchor or in a harbour, are not of high importance anymore. The performance of the controller and the results achieved will be further discussed in Section 5.

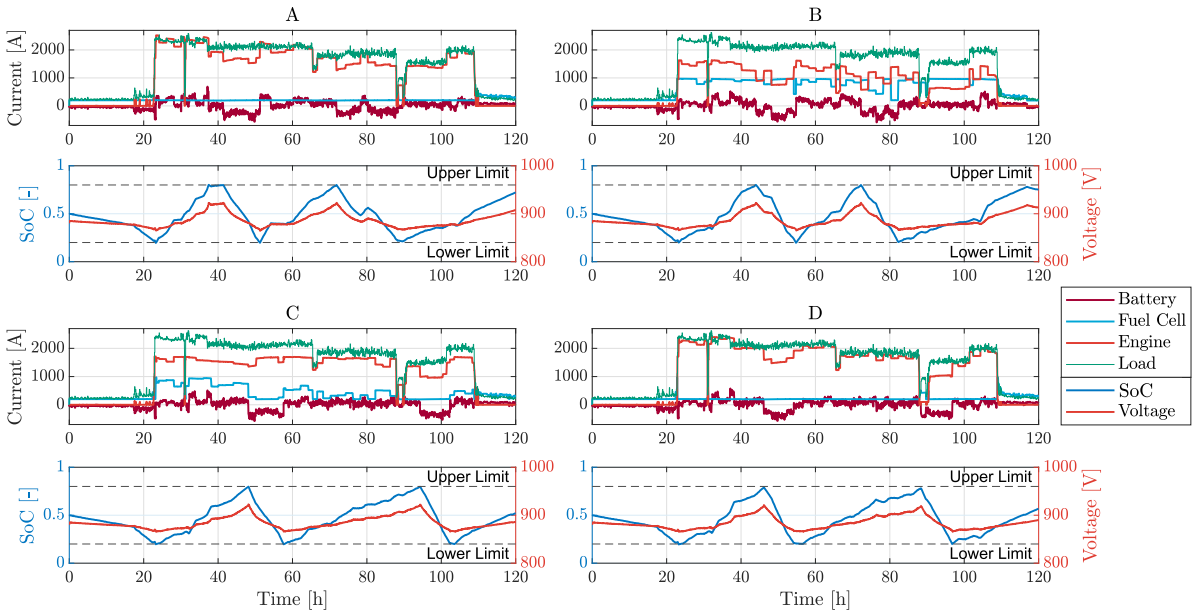

Fig. 15. Power balance, battery SOC and DC system voltage over 120 h of operation for SFC-Only ECMS (A), NOx-Only (B), full Pareto frontier ECMS (C) and mode-based Pareto frontier ECMS (D).

5. Results

This section analyzes the results of all scenarios. First, the single-objective optimization scenario is discussed, followed by the multi-objective scenarios including the Pareto frontier. Afterwards, all scenarios are compared with the two benchmarks B1 and B2 to showcase the potential for savings.

5.1. Simulation results

Fig. 15 provides an overview of the simulation results for all three ECMS scenarios showing the power balance, battery SOC and DC system voltage over 120 h of operation. In addition, a fourth scenario demonstrates operation with a single NOx reduction objective. While the control maintains the power balance in all scenarios, the resulting approach differs. In the SFC-Only (A) scenario, the ICE perform the main part of power tracking of the load, while the FC's are kept on a low operating point. This is mainly due to the respective high cost of hydrogen fuel compared to diesel. The ECMS formulation determines the power split between FCs, ICEs and batteries. Plot B shows the reference point of using a single NOx objective. The controller thus tries to minimize the use of diesel by using as much hydrogen as possible.

In plot C, the F-P scenario is shown, in which the multi-objective formulation selects the power generation based on the possible minimum, taking both objectives into account. In comparison to plot A, the FCs are used more to provide power in addition to the engines, which allows for less power generation with the engines. However, the FC are used at lower power than in the reference scenario B. The fourth scenario MB-P in plot D shows high similarity to SFC-Only ECMS (A) with the FCs on a constant low load, while the power tracking is mainly done with the engines. Both multi-objective scenarios (C & D) show similar battery behavior.

Battery behavior. Further, the battery behavior is examined more closely. In Fig. 16, the battery SOC and the DC system voltage of the MB-P scenario are shown over the 120 hr operating cycle, with a focus on a period of 15 h in the subplot. This focus illustrates that the battery is discharged in a time frame of multiple hours without high power ramps, which is believed to be helpful for the lifetime of the storage system. The complete overview of the operation reveals that over the course of the operation, the battery system is slowly charged and

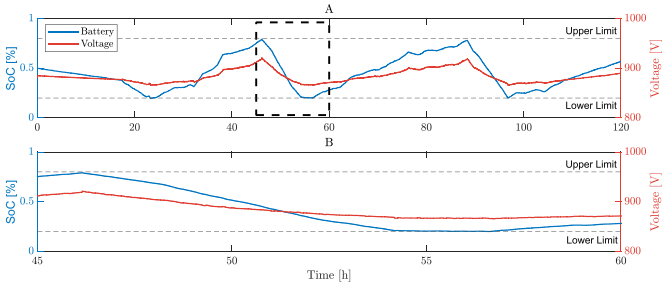

Fig. 16. Battery SOC and DC system voltage operating the system with the Mode-Based Pareto Scenario, including a 15 h zoom in of the battery operation (A: Full operation with a rectangular indicating the cut out, B: Zoom-in on the cut out).

discharged multiple times, making full use of the large storage. This allows for an optimization of the operating point of the ICE and the FC without stressing the battery system too much.

Pareto frontier. A central component of the weight determination process in the multi-objective formulation is the construction of a Pareto frontier. This approach enables a posteriori selection of weighting factors, allowing decision-makers to evaluate trade-offs between conflicting objectives after the set of optimal solutions has been generated. Although this method introduces a significant increase in computational effort — since the optimization problem must be solved repeatedly across the entire Pareto set — it offers valuable flexibility. By deferring the weighting decision to the post-processing stage, operators retain the ability to prioritize objectives based on real-world operational needs or policy preferences. The implications of this increased computational cost, as well as its trade-offs in terms of solution quality and decision transparency, will be further analyzed in the subsequent scenario comparison section.

First, the Pareto-Frontiers of the two multi-objective simulation scenarios are discussed in detail. For the weights of the objective function, a factor $\lambda \in [0,1]$ is introduced and the following relation $w_1 = \lambda$ and $w_2 = 1 - \lambda$ is established to highlight the necessary trade-off between adversarial objectives. In the hierarchical framework, the different cases of operation (FC-only, 1 Engine, 2 Engine) are examined with the Pareto-Frontier for each load setpoint. To highlight

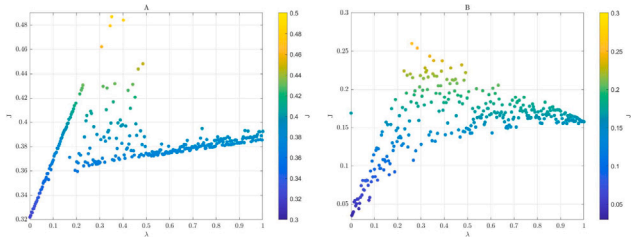

Fig. 17. Comparison of full Pareto frontier with 300 points with $w_1 = \lambda$ and $w_2 = 1 - \lambda$ (A: 1 Engine Scenario, B: 2 Engine Scenario).

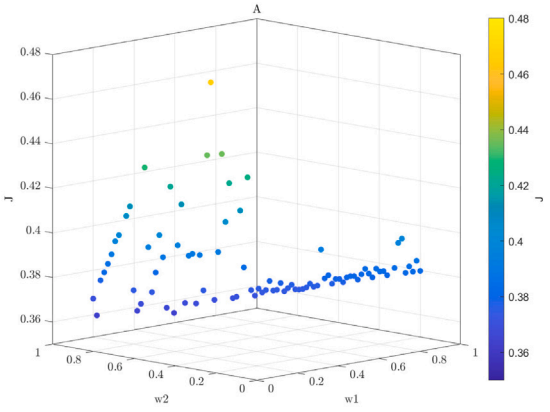

Fig. 18. Pareto frontier with 90 points in a 3D plot.

this, Fig. 17 shows a scatter plot of the Pareto frontier points for one step of the load profile (A: 1 Engine, B: 2 Engines) evaluated on their minimal objective function value achieved. In this, the Pareto frontier is investigated over 300 points for a close-up analysis of the solution space. The minimal objective function value J is shown on the y-axis and also indicated using a color scale, while the value of λ is shown on the x-axis. The first thing observable from this figure is that it highlights the difference in the minimal value achieved with choices of λ, even between λ-values with a high similarity. This illustrates the benefit achievable due to the introduction of the Pareto frontier. The second observation is that for the specific point of analysis, the operation of two engines side-by-side is more favorable than the use of just one engine. This is shown in the objective function values of subplot B, ranging from below 0.05 to a bit over 0.25, while the minimal value achieved in subplot A starts at 0.32. Therefore, the comparison of the two Pareto frontiers also helps to select the most suitable configuration in the hierarchical control framework.

To further highlight the variance in the solutions of the Pareto frontier, Fig. 18 shows a 3D-plot of the solution space of a 90 points investigation. This smaller solution space resembles more accurately a real-time application, where the computational time needs to be taken into account and Pareto frontiers with fewer points are more feasible. Also in this plot, it is observable that some weight combinations are greatly outperforming. However, the 3D representation shows that the optimal points are not necessarily to be found on the borders of the solution space. Further, it shows very clearly that, while many solutions are in the same range of minimal objective function value, significant outliers interrupt the space. Using those two figures, it demonstrates that employing the Pareto Frontier, a solution with a low overall objective function value and the case of operation at each time step can be picked.

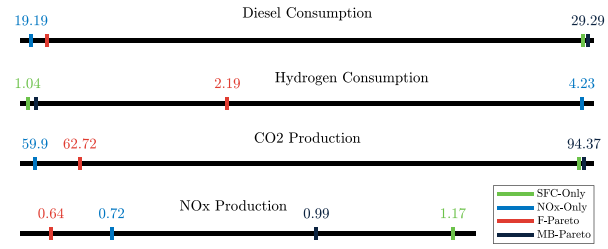

Fig. 19. Compromise between two factors in the parameters of diesel consumption, hydrogen consumption, CO_2 production and NO_x production, as well as the corresponding financial costs.

5.2. Scenario comparison

To estimate the performance of the proposed ECMS controller, all scenarios are compared to the two benchmarks presented in Section 4.2. However, while all ECMS scenarios produce valid control operations for the load profile, based on the choice of objectives, the operation will vary. To highlight this variety in the choice of optimal control operation, the performance is analyzed in more detail in the following. The performance of those scenarios can be evaluated based on the objectives of the optimization problem. In addition, the CO_2 emissions are established. Focusing on these aspects, the scenarios of Fig. 15 can be translated into the representation in Fig. 19. Each scenario is represented with a colored marker on a meter for the respective objective. It is directly observable that the value of the objective can vary drastically between the scenarios, however there is no scenario outperforming on all objectives which highlights the adversarial nature of the problem.

To examine the performance even further, the emissions are related to a financial factor to allow for a direct comparison of the total operational cost and compare them to the benchmark. The reference case for NOx-Only is disregarded in this, as it was mainly used to show the maximum possible hydrogen consumption and is not optimized to the same extent as the ECMS-scenarios. A full overview of the results is shown in Table 9. In this, the three ECMS scenarios (SFC-Only, F-P and MB-P) are shown alongside the benchmarks (B1, B2). Comparing the benchmarks B1 and B2, it shows that the retrofit to operate with hydrogen increases the cost of the operation drastically, while reducing emissions by more then 10 %. Moreover, emission reduction can be further increased by over 30 % for CO2 and over 40 % for NOx with advanced control.

Two scenarios (SFC, MB-P) achieve overall financial savings compared to the rule-based control of the retrofit B2. Those are achieved mainly by reducing hydrogen fuel consumption by a slight increase in diesel consumption. The other third scenario (F-P) shows an increase in the financial cost due to the increase in hydrogen consumption. However, the diesel consumption is even further reduced in this scenario. Analyzing NO_x emissions, the two scenarios (F-P, MB-P) employing multi-objective control manage to achieve drastic reductions (15 % - 45 %) in NO_x emissions. Furthermore, the F-P scenario also decreases CO_2 emissions by over 30 %, while both other scenarios increase the diesel consumption CO_2 emissions by a tiny margin. An interesting insight is also gained by comparing the two multi-objective scenarios. Employing the full Pareto frontier F-P results in a larger emission saving than the mode-based Pareto approach. This goes simultaneously with an increase in fuel cost, due to the high price of hydrogen. Employing an MB-P frontier approach provides results similar to the SFC-Only scenario. However, the scenario still saves nearly 15 % in NOx emissions. This demonstrates the savings potential from the choice of operational setpoint in the engine envelope. Further, the MB-P scenario resembles reality reasonably well, as operating at low load in port or at anchor often is correlated with high restrictions on emissions, while

Table 9
Scenario comparison.

	B1	B2	SFC	F-P	MB-P
Diesel [t]	34.5	28.72	29.20	19.47	29.29
Hydrogen [t]	-	1.16	1.04	2.19	1.09
CO_2 [t]	104.71	92.52	94.07	62.73	94.37
NO_x [t]	1.33	1.17	1.17	0.64	0.99
Fuel Cost [€]	27147	34888	34202	36850	34707
Change [%]			*-1.96*	*+5.62*	*-0.51*
CO_2 Cost [€]	9424	8327	8466	5646	8493
Change [%]			*+1.68*	*-32.2*	*+2*
NO_x Cost [€]	3000	2637	2655	1436	2260
Change [%]			*+0.63*	*-45.58*	*-14.36*
Total [€]	39571	45852	45323	43932	45460
Change [%]			*-1.15*	*-4.18*	*-0.85*

Table 10
Computational time for different Pareto frontier size.

Points	SFC	MB-P	F-P	F-P
	1	10	30	90
1 Engine and 4 Fuel Cells				
J_{min}	0.3893	0.3754	0.3657	0.3680
λ	1	0.6333	0.2655	0.3696
$1-\lambda$	0	0.3667	0.7345	0.6303
Time [s]	8.03	49.42	112.57	320.19
2 Engines and 4 Fuel Cells				
J_{min}	0.1573	0.1516	0.0817	0.0778
λ	1	0.6667	0.1	0.118
$1-\lambda$	0	0.3333	0.9	0.882
Time [s]	5.55	63.43	141.72	405.58

sailing is often in open waters, when SFC is of high importance, but emissions can be prioritized less.

Overall, all three scenarios decrease the price of operation in comparison to rule-based control. While the dual-fuel vessel operation is still more costly than the common industry-used diesel-electric approach, advanced control helps significantly in reducing cost. Especially the potential introduction of rates for carbon and other emissions in future, is likely to improve the financial feasibility of zero-emission fuels. Comparing the cheapest overall scenario to the B1 scenario highlights that over 30 % CO_2 and 45 % NO_x emissions can be saved at a limited cost increase. Furthermore, with increasing prices on conventional fuel and decreasing hydrogen prices in the future, this balance might shift further towards dual-fuel application.

Finally, the solution time of different versions of the Pareto frontier are investigated. In Table 10, an overview of four different scenarios is presented. All evaluate the same point using the same starting conditions. The SFC-Only scenario, which has pre-fixed weights, is compared with the solution of the MB-P scenario and a Pareto frontier approach with 30 and 90 points (F-P). A decrease in the minimized objective function value J_{min} can be observed with an increasing amount of points in the Pareto frontier. However, the computational time increases drastically as well. Therefore, it is possible to conclude that the choice of Pareto frontier size and design depends on the problem scenario, the required time frame and the available hardware.

Combining the results of those two tables, improvements can be seen compared to the RBC. The SFC-Only scenario with between 5 s and 10 s solution time per step, which solved the problem using a single-objective function, was able to reduce the economic cost of fuel consumption by 1.96 %, while only marginally increasing NOx emissions. As expected, using a Pareto frontier approach for the multi-objective objective function resulted in greater reduction of emissions at the cost of increased computational time. The large F-P (90 points) managed to achieve the highest savings in terms of NO_x reduction (over 45 %), mainly by increasing hydrogen consumption. However, the computational time of this size Pareto frontier would require a more potent machine to reduce the computational speed to feasible times. With the MB-P frontier of the size of 10 points, which had a pre-determined bias on the weights, it showed that it was possible to improve the performance in comparison to the SFC-Only scenario even further by saving nearly 15 % more NO_x while maintaining a reduction of fuel consumption (0.5 %). This scenario also showed drastically reduced computational time compared to the larger Pareto frontier tests, which showed an overall good performance.

6. Conclusion

In this paper, a novel Multi-Objective Equivalent Consumption Minimization Strategy control for vessels with electric propulsion and hybrid power supply using hydrogen fuel cells, diesel generators and battery energy storage was presented. The controller was developed to establish load sharing between these power sources for a mega-yacht, which was virtually retrofitted to accommodate two diesel generators, four hydrogen PEM fuel cells, and two battery packs. The system used a DC electrical distribution system, enabling variable speed operation of the diesel generators. To accurately represent the hybrid power system, measurements from laboratory engines and factory tests were used to create maps of the engines' specific fuel consumption and NO_x emissions, and the generator efficiency over the operational envelope. With the dual fuel set-up, the control challenge not only included the successful operation of multiple, heterogeneous components in parallel, but also presented the problem of the choice of operating fuel and its respective properties. For the multi-objective approach, it is focused on two non-correlated aspects: the economic cost of the fuel consumed and the NO_x emissions during operation. This provided a trade-off between emission-free hydrogen and cost, as hydrogen is significantly more expensive than diesel fuel. Overall, the resulting problem presented a non-convex, non-linear mixed-integer control challenge.

Based on this problem definition, the optimization problem is formulated as a hierarchical ECMS controller using a multi-start local optimization to allow for real-time optimization. The operation of the control algorithm was successfully demonstrated over 120 h of real-life operational data, chosen to represent multiple tasks of the vessel's operations. Two benchmark cases were considered to evaluate the performance of the proposed control strategy. The first represents an industry-standard reference, simulating a conventional diesel-electric vessel configuration equipped with four diesel generators managed by a power-tracking rule-based controller. The second benchmark involves the retrofitted version of the vessel using a rule-based controller tailored specifically to minimize specific fuel consumption. Unlike the proposed optimization-based approach, this single-objective controller operates with a fixed logic aimed solely at improving fuel efficiency without accounting for emissions or system-wide trade-offs. The ECMS controller was evaluated across three distinct scenarios to illustrate how different weight selections influence operational outcomes, reflecting potential preferences of the vessel operator. The first scenario implemented a single-objective ECMS focused exclusively on minimizing fuel consumption to demonstrate the optimal powersplitting. In the other scenarios, the full multi-objective capabilities of the ECMS were explored. These scenarios incorporated a Pareto frontier approach, enabling an a-posteriori selection of the objective function weights, thereby offering flexibility to prioritize either fuel cost or emissions depending on operational priorities. Moreover, the second scenario utilized a comprehensive Pareto frontier covering the entire trade-off space between economic cost and NO_x emissions. In contrast, the third scenario employed a reduced Pareto frontier confined to a narrower region, pre-biased by a specific operating mode. This allowed for faster computation while still capturing relevant trade-offs reflective of the selected operational context.

To evaluate the performance of the proposed control strategies, all scenarios — including the benchmarks — were systematically assessed based on two key metrics: total fuel consumption and the amount of NO_x emissions produced. The proposed multi-objective control strategy

demonstrated successful operation of the vessel across all scenarios, consistently outperforming the benchmark cases in terms of both fuel efficiency and emission reduction. Although integrating hydrogen into the energy mix leads to higher operational costs compared to a diesel-only configuration, the resulting emission reductions are substantial and highlight the environmental advantages of this approach. Moreover, all tested scenarios outperformed the second benchmark, i.e., the rule-based control of the retrofitted vessel, by delivering measurable reductions in operational costs. The SFC-only scenario achieved a reduction of nearly 2 % in fuel-related operational costs. Even greater benefits were observed in the multi-objective scenarios, demonstrating further improvements across economic and environmental performance indicators. Utilizing the full Pareto frontier enabled a reduction in NO_x emissions by more than 45 %, with only a marginal increase in operational costs relative to the rule-based control. Notably, the reduced Pareto frontier scenario outperformed the RBC approach across all evaluated metrics. In this scenario, the controller was able to still save 0.5 % in operational cost in comparison to the RBC, while reducing NO_x emission by nearly 15 %. This scenario was also computationally faster than using the full Pareto frontier approach due to a reduction in points investigated. The proposed multi-objective ECMS controller showed improvements in fuel economy and emission production aspects to current state-of-the-art approaches while not requiring any knowledge about the future due to instantaneous optimization.

The proposed multi-objective ECMS control strategy demonstrates promising performance for managing energy flows in dual-fuel fully electric vessels. Nonetheless, some limitations need to be addressed to enhance the realism, robustness, and industrial applicability of the approach. First, the present study is based on a quasi-steady-state simulation model that excludes transient behaviors of critical subsystems, including fuel cells, batteries, and power electronics. While suitable for long-term energy flow analysis and power-split optimization, this simplification neglects dynamic constraints such as ramp rates, system inertia, and control loop delays, which are vital for reliable real-time implementation. Future work should incorporate higher-fidelity dynamic models to assess and ensure controller feasibility under realistic operating conditions. Second, although the Pareto-based control formulation allows flexible trade-off analysis between fuel consumption and emissions, its real-time deployment poses computational challenges. The use of a reduced Pareto frontier mitigates this to some extent but still relies on pre-defined operational scenarios that may limit adaptability in unpredictable environments. Developing *adaptive and disturbance-aware control strategies* that preserve multi-objective performance while reducing online computational demand is a critical next step. Additionally, the current formulation optimizes instantaneous system states and does not consider voyage-level objectives. Integrating *time-preservation constraints* — e.g., arrival schedules or route completion times — would expand the controller's utility in mission-critical maritime operations. Third, the impact of component aging, particularly for batteries and fuel cells, has not been explicitly addressed. In practice, operational strategies significantly influence degradation trajectories, with implications for both cost and emissions over a vessel's lifetime. Future work should integrate *lifetime-aware control objectives* that co-optimize energy management and component health, potentially through data-driven or physics-informed degradation models.

Moreover, the current analysis is confined to a single vessel and operational profile. Broader validation across vessel classes, load scenarios, and environmental conditions is required to generalize the approach. Moreover, integrating this control framework into *early-stage vessel design* — for example, to support energy storage sizing or retrofit feasibility studies — would offer lifecycle-aware decision support for decarbonization. The estimated savings reported in this study underscore the potential of optimization-based control to drive efficiency gains in real-world maritime operations. As hydrogen prices decline and emissions pricing mechanisms become more widespread, the relevance of advanced energy management strategies will increase. Scaling this work to full-voyage simulations and experimental testbeds will be essential for demonstrating operational readiness and supporting the transition to low-emission shipping.

CRediT authorship contribution statement

Charlotte Löffler: Writing – review & editing, Writing – original draft, Visualization, Validation, Methodology, Investigation, Formal analysis, Data curation, Conceptualization. **Rinze Geertsma:** Writing – review & editing, Validation, Supervision, Conceptualization. **Henk Polinder:** Writing – review & editing, Supervision, Resources, Project administration, Funding acquisition. **Andrea Coraddu:** Writing – review & editing, Validation, Supervision, Resources, Project administration, Methodology, Funding acquisition, Conceptualization.

Declaration of competing interest

The authors declare that they have no known competing financial interests or personal relationships that could have appeared to influence the work reported in this paper.

Acknowledgments

This research is supported by the project MENENS, funded by the Netherlands Enterprise Agency (RVO) under the grant number MOB21012.

Data availability

The authors do not have permission to share data.

References

[1] IPCC, Masson-Delmotte V, Zhai P, Pirani A, Connors SL, Péan C, et al., editors. Climate Change 2021: The Physical Science Basis. Contribution of Working Group I to the Sixth Assessment Report of the Intergovernmental Panel on Climate Change. Cambridge University Press. In Press; 2021.
[2] IEA. World energy outlook 2021, IEA, Paris. 2021.
[3] Eyring V, Köhler HW, van Aardenne J, Lauer A. Emissions from international shipping: 1. The last 50 years. J Geophys Res: Atmospheres 2005;110(D17). http://dx.doi.org/10.1029/2004JD005619.
[4] IMO Uk. Fourth IMO GHG Study 2020 - Full report and annexes.pdf. 2020.
[5] IMO Uk, Smith TWP, Jalkanen JP, Anderson BA, Corbett JJ, Faber J, et al. The third IMO GHG Study 2014. 2015.
[6] Dalsøren SB, Eide MS, Endresen Ø, Mjelde A, Gravir G, Isaksen ISA. Update on emissions and environmental impacts from the international fleet of ships: The contribution from major ship types and ports. Atmospheric Chem Phys 2009;9(6):2171–94. http://dx.doi.org/10.5194/acp-9-2171-2009.
[7] Eyring Veronika, Isaksen Ivar SA, Berntsen Terje, Collins William J, Corbett James J, Endresen Oyvind, et al. Transport impacts on atmosphere and climate: Shipping. In: Transport impacts on atmosphere and climate: The aTTICA assessment report, Atmos Environ In: Transport impacts on atmosphere and climate: The aTTICA assessment report, 2010;44(37):4735–71.http://dx.doi.org/10.1016/j.atmosenv.2009.04.059,
[8] Endresen Øyvind, Sørgård Eirik, Sundet Jostein K, Dalsøren Stig B, Isaksen Ivar SA, Berglen Tore F, et al. Emission from international sea transportation and environmental impact. J Geophys Res: Atmospheres 2003;108(D17). http://dx.doi.org/10.1029/2002JD002898.
[9] Eyring V, Köhler HW, Lauer A, Lemper B. Emissions from international shipping: 2. Impact of future technologies on scenarios until 2050. J Geophys Res: Atmospheres 2005;110(D17). http://dx.doi.org/10.1029/2004JD005620.
[10] Hansen Jan Fredrik, Wendt Frank. History and state of the art in commercial electric ship propulsion, integrated power systems, and future trends. Proc IEEE 2015;103(12):2229–42. http://dx.doi.org/10.1109/JPROC.2015.2458990.
[11] Geertsma RD, Negenborn RR, Visser K, Hopman JJ. Design and control of hybrid power and propulsion systems for smart ships: A review of developments. Appl Energy 2017;194:30–54. http://dx.doi.org/10.1016/j.apenergy.2017.02.060.
[12] Jaurola Miikka, Hedin Anders, Tikkanen Seppo, Huhtala Kalevi. Optimising design and power management in energy-efficient marine vessel power systems: A literature review. J Mar Eng Technol 2019;18(2):92–101. http://dx.doi.org/10.1080/20464177.2018.1505584.
[13] Korberg AD, Brynolf S, Grahn M, Skov IR. Techno-economic assessment of advanced fuels and propulsion systems in future fossil-free ships. Renew Sustain Energy Rev 2021;142:110861. http://dx.doi.org/10.1016/j.rser.2021.110861.
[14] Perčić Maja, Ančić Ivica, Vladimir Nikola. Life-cycle cost assessments of different power system configurations to reduce the carbon footprint in the Croatian short-sea shipping sector. Renew Sustain Energy Rev 2020;131:110028. http://dx.doi.org/10.1016/j.rser.2020.110028.

[15] Barone Giovanni, Buonomano Annamaria, Del Papa Gianluca, Maka Robert, Palombo Adolfo. Approaching zero emissions in ports: Implementation of batteries and supercapacitors with smart energy management in hybrid ships. Energy Convers Manage 2024;314:118446. http://dx.doi.org/10.1016/j.enconman.2024.118446.

[16] Stančin H, Mikulčić H, Wang X, Duić N. A review on alternative fuels in future energy system. Renew Sustain Energy Rev 2020;128:109927. http://dx.doi.org/10.1016/j.rser.2020.109927.

[17] Law Li Chin, Foscoli Beatrice, Mastorakos Epaminondas, Evans Stephen. A comparison of alternative fuels for shipping in terms of lifecycle energy and cost. Energies 2021;14(24):8502. http://dx.doi.org/10.3390/en14248502.

[18] Deniz Cengiz, Zincir Burak. Environmental and economical assessment of alternative marine fuels. J Clean Prod 2016;113:438–49. http://dx.doi.org/10.1016/j.jclepro.2015.11.089.

[19] Sharma Nawin Ranjan, Dimitrios, Dalaklis, Olcer Aykut I, Nikitakos, Nikitas. LNG a clean fuel – the underlying potential to improve thermal efficiency. J Mar Eng Technol 2022;21(2):111–24. http://dx.doi.org/10.1080/20464177.2020.1827491.

[20] Kim Siwoong, Oh Seunghun, Kang Sanggyu. Techno-economic assessment of liquefied hydrogen tanker ships utilizing various propulsion systems. Energy Convers Manage 2025;336:119895. http://dx.doi.org/10.1016/j.enconman.2025.119895.

[21] Livanos George A, Theotokatos Gerasimos, Pagonis Dimitrios-Nikolaos. Techno-economic investigation of alternative propulsion plants for Ferries and RoRo ships. Energy Convers Manage 2014;79:640–51. http://dx.doi.org/10.1016/j.enconman.2013.12.050.

[22] Trivyza Nikoletta L, Rentizelas Athanasios, Theotokatos Gerasimos. A novel multi-objective decision support method for ship energy systems synthesis to enhance sustainability. Energy Convers Manage 2018;168:128–49. http://dx.doi.org/10.1016/j.enconman.2018.04.020.

[23] Prussi M, Scarlat N, Acciaro M, Kosmas V. Potential and limiting factors in the use of alternative fuels in the European maritime sector. J Clean Prod 2021;291:125849. http://dx.doi.org/10.1016/j.jclepro.2021.125849.

[24] Scappin Fabio, Stefansson Sigurdur H, Haglind Fredrik, Andreasen Anders, Larsen Ulrik. Validation of a zero-dimensional model for prediction of NOx and engine performance for electronically controlled marine two-stroke diesel engines. Appl Therm Eng 2012;37:344–52. http://dx.doi.org/10.1016/j.applthermaleng.2011.11.047.

[25] Geertsma RD, Negenborn RR, Visser K, Loonstijn MA, Hopman JJ. Pitch control for ships with diesel mechanical and hybrid propulsion: Modelling, validation and performance quantification. Appl Energy 2017;206:1609–31. http://dx.doi.org/10.1016/j.apenergy.2017.09.103.

[26] Zahedi Bijan, Norum Lars E, Ludvigsen Kristine B. Optimized efficiency of all-electric ships by Dc hybrid power systems. J Power Sources 2014;255:341–54. http://dx.doi.org/10.1016/j.jpowsour.2014.01.031.

[27] Nuchturee Chalermkiat, Li Tie, Xia Hongpu. Energy efficiency of integrated electric propulsion for ships – A review. Renew Sustain Energy Rev 2020;134:110145. http://dx.doi.org/10.1016/j.rser.2020.110145.

[28] Kalikatzarakis M, Geertsma RD, Boonen EJ, Visser K, Negenborn RR. Ship energy management for hybrid propulsion and power supply with shore charging. Control Eng Pract 2018;76:133–54. http://dx.doi.org/10.1016/j.conengprac.2018.04.009.

[29] Nema Pragya, Nema RK, Rangnekar Saroj. A current and future state of art development of hybrid energy system using wind and PV-solar: A review. Renew Sustain Energy Rev 2009;13(8):2096–103. http://dx.doi.org/10.1016/j.rser.2008.10.006.

[30] Park Hyeongjun, Sun Jing, Pekarek Steven, Stone Philip, Opila Daniel, Meyer Richard, et al. Real-time model predictive control for shipboard power management using the IPA-SQP Approach. IEEE Trans Control Syst Technol 2015;23(6):2129–43. http://dx.doi.org/10.1109/TCST.2015.2402233.

[31] Johannesson Lars, Murgovski Nikolce, Jonasson Erik, Hellgren Jonas, Egardt Bo. Predictive energy management of hybrid long-haul trucks. Control Eng Pract 2015;41:83–97. http://dx.doi.org/10.1016/j.conengprac.2015.04.014.

[32] Unger Johannes, Kozek Martin, Jakubek Stefan. Nonlinear model predictive energy management controller with load and cycle prediction for non-road HEV. Control Eng Pract 2015;36:120–32. http://dx.doi.org/10.1016/j.conengprac.2014.12.001.

[33] Kermani S, Delprat S, Guerra TM, Trigui R, Jeanneret B. Predictive energy management for hybrid vehicle. In: Special section: IFAC symposium on advanced control of chemical processes - ADCHEM 2009, Control Eng Pract In: Special section: IFAC symposium on advanced control of chemical processes - ADCHEM 2009, 2012;20(4):408–20.http://dx.doi.org/10.1016/j.conengprac.2011.12.001,

[34] Pozzato Gabriele, Müller Matthias, Formentin Simone, Savaresi Sergio M. Economic MPC for online least costly energy management of hybrid electric vehicles. Control Eng Pract 2020;102:104534. http://dx.doi.org/10.1016/j.conengprac.2020.104534.

[35] Vu Tuyen Van, Gonsoulin David, Diaz Fernand, Edrington Chris S, El-Mezyani Touria. Predictive control for energy management in ship power systems under high-power ramp rate loads. IEEE Trans Energy Convers 2017;32(2):788–97. http://dx.doi.org/10.1109/TEC.2017.2692058.

[36] Rodriguez Rusber, F. Trovão João Pedro, Solano Javier. Fuzzy logic-model predictive control energy management strategy for a dual-mode locomotive. Energy Convers Manage 2022;253:115111. http://dx.doi.org/10.1016/j.enconman.2021.115111.

[37] Ma Mengcheng, Hu Jianjun, Xiao Renhua. Energy management strategy with model prediction for fuel cell hybrid trucks considering vehicle mass and road slope. Energy Convers Manage 2025;333:119791. http://dx.doi.org/10.1016/j.enconman.2025.119791.

[38] Haseltalab Ali, Negenborn Rudy R. Model predictive maneuvering control and energy management for all-electric autonomous ships. Appl Energy 2019;251:113308. http://dx.doi.org/10.1016/j.apenergy.2019.113308.

[39] Jiang Jundao, Zou Liang, Liu Xingdou, Han Zhiyun, Wang Rui. A two-level real-time energy management strategy incorporating load forecasting for hydrogen fuel cell-powered ships. Energy Convers Manage 2025;341:120032. http://dx.doi.org/10.1016/j.enconman.2025.120032.

[40] Sturzenegger David, Gyalistras Dimitrios, Morari Manfred, Smith Roy S. Model predictive climate control of a swiss office building: Implementation, results, and cost–benefit analysis. IEEE Trans Control Syst Technol 2016;24(1):1–12. http://dx.doi.org/10.1109/TCST.2015.2415411.

[41] Paganelli G, Delprat S, Guerra TM, Rimaux J, Santin JJ. Equivalent consumption minimization strategy for parallel hybrid powertrains. In: Vehicular technology conference. IEEE 55th vehicular technology conference. VTC spring 2002 (cat. no.02CH37367). 4, 2002, p. 2076–81. http://dx.doi.org/10.1109/VTC.2002.1002989.

[42] Torreglosa JP, Jurado F, García P, Fernández LM. Hybrid fuel cell and battery tramway control based on an equivalent consumption minimization strategy. Control Eng Pract 2011;19(10):1182–94. http://dx.doi.org/10.1016/j.conengprac.2011.06.008.

[43] Zhang Wenbin, Li Jianqiu, Xu Liangfei, Ouyang Minggao. Optimization for a fuel cell/battery/capacity tram with equivalent consumption minimization strategy. Energy Convers Manage 2017;134:59–69. http://dx.doi.org/10.1016/j.enconman.2016.11.007.

[44] Chasse A, Sciarretta A. Supervisory control of hybrid powertrains: An experimental benchmark of offline optimization and online energy management. Control Eng Pract 2011;19(11):1253–65. http://dx.doi.org/10.1016/j.conengprac.2011.04.008.

[45] Sciarretta A, Serrao L, Dewangan PC, Tona P, Bergshoeff END, Bordons C, et al. A control benchmark on the energy management of a plug-in hybrid electric vehicle. Control Eng Pract 2014;29:287–98. http://dx.doi.org/10.1016/j.conengprac.2013.11.020.

[46] Li Huan, Ravey Alexandre, N'Diaye Abdoul, Djerdir Abdesslem. A novel equivalent consumption minimization strategy for hybrid electric vehicle powered by fuel cell, battery and supercapacitor. J Power Sources 2018;395:262–70. http://dx.doi.org/10.1016/j.jpowsour.2018.05.078.

[47] Li Huan, Ravey Alexandre, N'Diaye Abdoul, Djerdir Abdesslem. Online adaptive equivalent consumption minimization strategy for fuel cell hybrid electric vehicle considering power sources degradation. Energy Convers Manage 2019;192:133–49. http://dx.doi.org/10.1016/j.enconman.2019.03.090.

[48] Lei Zhenzhen, Qin Datong, Hou Liliang, Peng Jingyu, Liu Yonggang, Chen Zheng. An adaptive equivalent consumption minimization strategy for plug-in hybrid electric vehicles based on traffic information. Energy 2020;190:116409. http://dx.doi.org/10.1016/j.energy.2019.116409.

[49] García P, Torreglosa JP, Fernández LM, Jurado F. Viability study of a FC-battery-SC tramway controlled by equivalent consumption minimization strategy. Int J Hydrog Energy 2012;37(11):9368–82. http://dx.doi.org/10.1016/j.ijhydene.2012.02.184.

[50] Nüesch Tobias, Cerofolini Alberto, Mancini Giorgio, Cavina Nicolò, Onder Christopher, Guzzella Lino. Equivalent consumption minimization strategy for the control of real driving NOx emissions of a diesel hybrid electric vehicle. Energies 2014;7(5):3148–78. http://dx.doi.org/10.3390/en7053148.

[51] Li Jie, Liu Yonggang, Qin Datong, Li Guang, Chen Zheng. Research on equivalent factor boundary of equivalent consumption minimization strategy for PHEVs. IEEE Trans Veh Technol 2020;69(6):6011–24. http://dx.doi.org/10.1109/TVT.2020.2986541.

[52] Löffler Charlotte, Kopka Timon, Geertsma Rinze, Polinder Henk, Coraddu Andrea. Optimizing energy management for full-electric vessels: A health-aware approach with hydrogen and diesel employing equivalent consumption minimization strategy. In: 2023 IEEE transportation electrification conference and expo, Asia-Pacific (ITEC Asia-Pacific). Chiang Mai, Thailand: IEEE; 2023, p. 1–8. http://dx.doi.org/10.1109/ITECAsia-Pacific59272.2023.10372270.

[53] Löffler Charlotte, Geertsma Rinze, Mitropoulou Despoina, Polinder Henk, Coraddu Andrea. Equivalent consumption minimization strategy for full-electric ship energy management with multiple objectives. In: Modelling and optimisation of ship energy systems 2023. 2024, http://dx.doi.org/10.59490/moses.2023.673.

[54] Broer Annabel, Polinder Henk, van Biert Lindert. Polymer electrolyte membrane fuel cell degradation in ships — Review of degradation mechanisms and research gaps. J Power Sources 2025;640:236678. http://dx.doi.org/10.1016/j.jpowsour.2025.236678.

[55] Vasilikis NI, Geertsma RD, Visser K. Operational data-driven energy performance assessment of ships: The case study of a naval vessel with hybrid propulsion. J Mar Eng Technol 2022;1–17. http://dx.doi.org/10.1080/20464177.2022.2058690.
[56] Vasilikis Nikolaos, Geertsma Rinze, Coraddu Andrea. A digital twin approach for maritime carbon intensity evaluation accounting for operational and environmental uncertainty. Ocean Eng 2023;288:115927. http://dx.doi.org/10.1016/j.oceaneng.2023.115927.
[57] Tremblay Olivier, Dessaint Louis-A, Dekkiche Abdel-Illah. A generic battery model for the dynamic simulation of hybrid electric vehicles. In: 2007 IEEE vehicle power and propulsion conference. 2007, p. 284–9. http://dx.doi.org/10.1109/VPPC.2007.4544139.
[58] Shepherd CM. Design of primary and secondary cells: II . an equation describing battery discharge. J Electrochem Soc 1965;112(7):657. http://dx.doi.org/10.1149/1.2423659.
[59] Campagna Nicola, Castiglia Vincenzo, Miceli Rosario, Mastromauro Rosa Anna, Spataro Ciro, Trapanese Marco, et al. Battery models for battery powered applications: A comparative study. Energies 2020;13(16):4085. http://dx.doi.org/10.3390/en13164085.
[60] Wang Yujie, Tian Jiaqiang, Sun Zhendong, Wang Li, Xu Ruilong, Li Mince, et al. A comprehensive review of battery modeling and state estimation approaches for advanced battery management systems. Renew Sustain Energy Rev 2020;131:110015. http://dx.doi.org/10.1016/j.rser.2020.110015.
[61] Li Shuhui, Ke Bao. Study of battery modeling using mathematical and circuit oriented approaches. In: 2011 IEEE power and energy society general meeting. 2011, p. 1–8. http://dx.doi.org/10.1109/PES.2011.6039230.
[62] Haraldsson Kristina, Wipke Keith. Evaluating PEM fuel cell system models. J Power Sources 2004;126(1):88–97. http://dx.doi.org/10.1016/j.jpowsour.2003.08.044.
[63] Pasricha S, Shaw SR. A dynamic PEM fuel cell model. IEEE Trans Energy Convers 2006;21(2):484–90. http://dx.doi.org/10.1109/TEC.2005.860402.
[64] Abdin Z, Webb CJ, Gray E MacA. PEM fuel cell model and simulation in Matlab–Simulink based on physical parameters. Energy 2016;116:1131–44. http://dx.doi.org/10.1016/j.energy.2016.10.033.
[65] Baschuk JJ, Li Xianguo. A general formulation for a mathematical PEM fuel cell model. J Power Sources 2005;142(1):134–53. http://dx.doi.org/10.1016/j.jpowsour.2004.09.027.
[66] Shan Yuyao, Choe Song-Yul. A high dynamic PEM fuel cell model with temperature effects. J Power Sources 2005;145(1):30–9. http://dx.doi.org/10.1016/j.jpowsour.2004.12.033.
[67] Souleman Njoya M, Tremblay Olivier, Dessaint Louis-A. A generic fuel cell model for the simulation of fuel cell power systems. In: 2009 IEEE power & energy society general meeting. 2009, p. 1–8. http://dx.doi.org/10.1109/PES.2009.5275853.
[68] Feiner A-S, McEvoy AJ. The Nernst Equation. J Chem Educ 1994;71(6):493. http://dx.doi.org/10.1021/ed071p493.
[69] Barbir Frano. PEM fuel cells: Theory and practice. Academic Press; 2012.
[70] Nedstack FCS 13-XXL Pem FC stack. 2019.
[71] Zeleznik Frank J, McBride Bonnie J. Modeling the Internal Combustion Engine.
[72] Pariotis EG, Kosmadakis GM, Rakopoulos CD. Comparative analysis of three simulation models applied on a motored internal combustion engine. In: Special issue of energy conversion and management dedicated to ECOS 2011 - the 24th international conference on efficiency, costs, optimization, simulation and environmental impact of energy systems, Energy Convers Manage In: Special issue of energy conversion and management dedicated to ECOS 2011 - the 24th international conference on efficiency, costs, optimization, simulation and environmental impact of energy systems, 2012;60:45–55.http://dx.doi.org/10.1016/j.enconman.2011.11.031,
[73] Krause PC, Wasynczjk O. Analysis of electric machinery [Books and Reports]. IEEE Power Eng Rev 1995;15(3):40. http://dx.doi.org/10.1109/MPER.1995.365078.
[74] Fitzgerald Arthur Ernest, Kingsley Charles, Umans Stephen D. Electric machinery, 6th ed.. mcGraw-hill series in electrical and computer engineering, Boston, Mass.: McGraw-Hill; 2009, international ed., [Nachdr.].
[75] Marti JR, Louie KW. A phase-domain synchronous generator model including saturation effects. IEEE Trans Power Syst 1997;12(1):222–9. http://dx.doi.org/10.1109/59.574943.
[76] Rawlings James Blake, Mayne David Q, Diehl Moritz. Model predictive control: Theory, computation, and design. 2nd ed.. Madison, Wisconsin: Nob Hill Publishing; 2017.
[77] Floudas Christodoulos A. Nonlinear and mixed-integer optimization: Fundamentals and applications. Oxford University Press; 1995.
[78] Roberts AW. CHAPTER 4.2 - convex functions. In: Gruber PM, Wills JM, editors. Handbook of convex geometry. Amsterdam: North-Holland; 1993, p. 1081–104. http://dx.doi.org/10.1016/B978-0-444-89597-4.50013-5.
[79] Ekeland Ivar. Nonconvex minimization problems. Bull Am Math Soc 1979;1(3):443–74. http://dx.doi.org/10.1090/S0273-0979-1979-14595-6.
[80] Burer Samuel, Letchford Adam N. Non-convex mixed-integer nonlinear programming: A survey. Surv Oper Res Manag Sci 2012;17(2):97–106. http://dx.doi.org/10.1016/j.sorms.2012.08.001.
[81] El-Bakry AS, Tapia RA, Tsuchiya T, Zhang Y. On the formulation and theory of the Newton interior-point method for nonlinear programming. J Optim Theory Appl 1996;89(3):507–41. http://dx.doi.org/10.1007/BF02275347.
[82] Boggs Paul T, Tolle Jon W. Sequential Quadratic Programming. Acta Numer 1995;4:1–51. http://dx.doi.org/10.1017/S0962492900002518.
[83] Winnes Hulda, Fridell Erik, Yaramenka Katarina, Nelissen Dagmar. NOx Controls for Shipping in EU Seas. Technical report.